JGR Biogeosciences

RESEARCH ARTICLE
10.1029/2024JG008144

Influence of Organo-Mineral Associations on Terrestrial Particulate Organic Matter Dispersal in the Northern Gulf of Mexico

Yord W. Yedema[1], Francesca Sangiorgi[1], João P. Trabucho-Alexandre[1], Klaas G. J. Nierop[1], Jorien E. Vonk[2], and Francien Peterse[1]

[1]Department of Earth Sciences, Utrecht University, Utrecht, The Netherlands, [2]Department of Earth Sciences, Vrije Universiteit Amsterdam, Amsterdam, The Netherlands

Key Points:

- We investigate the influence of organo-mineral associations on the transport of terrestrial organic matter (TerrOM) in the marine realm
- Plant-derived OM has a higher affinity with mineral surfaces than freshwater and soil-microbial OM
- Differences in the stability of organo-mineral associations per TerrOM type can explain their differential dispersal in the Gulf of Mexico

Correspondence to:
Y. W. Yedema,
y.w.ijedema@uu.nl

Citation:
Yedema, Y. W., Sangiorgi, F., Trabucho-Alexandre, J. P., Nierop, K. G. J., Vonk, J. E., & Peterse, F. (2024). Influence of organo-mineral associations on terrestrial particulate organic matter dispersal in the northern Gulf of Mexico. *Journal of Geophysical Research: Biogeosciences*, *129*, e2024JG008144. https://doi.org/10.1029/2024JG008144

Received 15 MAR 2024
Accepted 17 OCT 2024

Author Contributions:
Conceptualization: Yord W. Yedema, Francesca Sangiorgi, Francien Peterse
Data curation: João P. Trabucho-Alexandre
Formal analysis: Yord W. Yedema, João P. Trabucho-Alexandre, Klaas G. J. Nierop, Jorien E. Vonk
Investigation: Yord W. Yedema, Francien Peterse
Methodology: Yord W. Yedema, Francesca Sangiorgi, João P. Trabucho-Alexandre, Klaas G. J. Nierop, Jorien E. Vonk, Francien Peterse
Resources: João P. Trabucho-Alexandre
Supervision: Francesca Sangiorgi, Francien Peterse
Validation: Francesca Sangiorgi
Visualization: Yord W. Yedema
Writing – original draft: Yord W. Yedema

Abstract We investigate the influence of organo-mineral associations on the dispersal of terrestrial organic matter (TerrOM) along a land-sea transect offshore the Atchafalaya river in the northern Gulf of Mexico (GoM). We analyzed bulk sediment properties, mineral surface area, and clay composition and used lipid biomarkers to distinguish plant-derived (long-chain *n*-alkanes and *n*-alcohols) freshwater aquatic (C_{32} 1,15-diols) and soil-microbial (branched glycerol dialkyl glycerol tetraethers (brGDGTs)) OM-pools in different grain size fractions (≥250, 250–125, 125–63, 63–30, 30–10 and <10 μm) of marine surface sediments. Concentrations and mineral loadings of the targeted biomarkers were highest in the <30 μm fractions, suggesting an affinity with clay minerals. Spatially, concentrations of higher plant-derived *n*-alkanes remained relatively constant along the transect, whereas those of the other OM-pools rapidly decreased further offshore. This suggests that the association of plant-derived OM with mineral surfaces is better maintained than that of freshwater and soil-microbial OM. In addition, similar distributions among grain size fractions at each site for the C_{32} 1,15-diols and brGDGTs suggest that these compounds are likely not associated with mineral surfaces in the marine realm. Furthermore, as TerrOM might be stripped from mineral surfaces upon discharge in the marine realm, the dispersal of TerrOM-pools could also represent a degradation signal, as *n*-alkanes are more resistant than long-chain diols and brGDGTs. Together, our results indicate that the stability of organo-mineral associations in the marine realm differs per TerrOM-pool and can lead to a differential dispersal of these pools, and thus OM sequestration patterns in the northern GoM.

Plain Language Summary Terrestrially derived organic matter (TerrOM) can form bonds with mineral surfaces, which protect it against degradation during its journey to the marine realm. However, it is unclear whether these bonds persist after fluvial transport and discharge into the ocean, which has implications for the burial efficiency of TerrOM in coastal zones. In this study, we investigate the influence of these bonds between TerrOM and mineral surfaces on the dispersal of different TerrOM pools (plant, freshwater aquatic, and soil-microbial OM) in the northern Gulf of Mexico by analyzing grain size fractions of marine surface sediments along a land-sea transect offshore the Atchafalaya river. We find that higher plant-derived OM is protected against degradation by mineral surfaces, whereas freshwater and soil-microbial OM rapidly decrease further offshore. The low concentrations of freshwater aquatic and soil-microbial OM associated with mineral surfaces suggests that these TerrOM pools are likely not protected during transport and therefore rapidly remineralized once they reach the ocean.

1. Introduction

The burial of terrestrial organic matter (TerrOM) in marine sediments is a key step in the global carbon cycle, as it represents a long-term sink for photosynthetically fixed atmospheric CO_2. In particular, river-dominated continental shelves receive large amounts of fluvially discharged TerrOM and are, therefore, considered a hotspot for OM burial (Berner, 1982; Bianchi et al., 2018). The amount of TerrOM that is ultimately buried in continental shelf sediments correlates well with the relative contribution of silt- and clay-size minerals (Bergamaschi et al., 1997; Coppola et al., 2007; Kennedy & Wagner, 2011; Ransom et al., 1998). It is, therefore, generally assumed that TerrOM is protected against degradation in the marine realm through associations with surfaces of clays and reactive iron minerals (Hemingway et al., 2019; Keil et al., 1994a; Lalonde et al., 2012; Mayer, 1994a, 1994b; Zhao et al., 2018).

Writing – review & editing: Francesca Sangiorgi, João P. Trabucho-Alexandre, Klaas G. J. Nierop, Jorien E. Vonk, Francien Peterse

Associations of TerrOM with mineral surfaces initially form in soils, which make the OM more persistent against degradation than non-bound particulate OM (Kögel-Knabner et al., 2008; Lavallee et al., 2020; Von Lützow et al., 2006). The type and strength of the organo-mineral bonds and thus the preservation of OM depend on the mineralogy and the composition of the OM. For example, minerals can vary in their surface area (SA), cation exchange capacity (i.e., the capacity of minerals to form organo-mineral bonds via cation-bridging), and inter-layer expansion ability, which influence the amount of OM that can bond to a mineral surface (Blattmann et al., 2019; Carroll, 1959). Similarly, the nature of functional groups of the OM can play a role in the type of bond that is formed and thus the strength of the association (Keil & Mayer, 2014; Zhou et al., 1994). Although mineral-associated OM in soils generally consists of about equal amounts of microbial and plant-delivered OM (Angst et al., 2021), it is not yet fully known to which extent these associations persist during fluvial transport, discharge into the marine realm, and subsequent burial on the seafloor (Blattmann et al., 2019; Hedges & Oades, 1997; Keil & Mayer, 2014). For instance, TerrOM appears to be progressively lost from mineral surfaces during river transport (e.g., Freymond et al., 2018; Keil et al., 1997; Repasch et al., 2022), although flume experiments suggest that OM loss is in fact limited during fluvial transport and primarily occurs during (temporary) floodplain storage (Scheingross et al., 2019). Furthermore, during the transition from fresh to saline water, TerrOM can be decoupled from mineral surfaces as a result of changes in ion concentration (Brockamp, 2011; Chen et al., 2020) and pH (Theng, 2012), leading to a decrease in mineral-associated TerrOM with increasing distance from shore (e.g., Bröder et al., 2016, 2018; Hou et al., 2020; Mayer, 1994b; Yu et al., 2021). Hence, instead of reaching the seafloor, part of the TerrOM delivered to the coastal zone is remineralized in the water column, releasing carbon back to the atmosphere (Blair & Aller, 2012; Hedges et al., 1997; LaRowe et al., 2020). For example, only 20%–50% of the particulate organic carbon flux from the Mississippi and Atchafalaya Rivers (MAR) that transport large amounts of TerrOM to the northern Gulf of Mexico (GoM) is estimated to be buried on the Louisiana shelf (Trefry et al., 1994). In addition, TerrOM can be differentially distributed over grain size and/or density fractions (Angst et al., 2017; Hedges & Oades, 1997), which make the transport of these OM components susceptible to hydraulic sorting. For example, lignin derived from C4 grasses in the upper Mississippi basin was found farther offshore in the GoM than plant detritus derived from coastal C3 forests and swamps due to the association of C4 plant material with fine fraction sediments, facilitating its offshore transport (Goñi et al., 1997). Similarly, lignin and bacteriohopanepolyol ratios varied between density fractions of northern GoM surface sediments, suggesting preferential preservation and sorting of these compounds by certain density fractions (Kusch et al., 2019; Sampere et al., 2008; Wakeham et al., 2009).

We have recently shown that after discharge by the MAR, soil-microbial, freshwater aquatic-produced, and plant-derived OM were dispersed differently in the northern GoM; where the first two pools were rapidly lost upon entering the marine realm, plant-derived OM was transported further off- and along shore (Yedema et al., 2023). Here, we aim to constrain whether different associations with mineral surfaces can explain the distinct dispersal patterns of these TerrOM types in GoM sediments. The TerrOM pools are distinguished based on long-chain *n*-alkanes, *n*-alcohols, C_{32} 1,15-diols, and branched glycerol dialkyl glycerol tetraethers (brGDGTs). Specifically, odd-carbon-numbered long-chain *n*-alkanes (C_{29}–C_{35}) are part of leaf waxes of vascular plants. Their relatively good resistance against oxic degradation makes them suitable tracers of plant OM in the marine environment (Eglinton & Hamilton, 1967). Similarly, long-chain *n*-alcohols (C_{22}–C_{28}) are also derived from terrestrial plants (Eglinton & Hamilton, 1967). Long-chain (>C_{28}) diols generally occur in marine settings and are produced by marine eustigmatophyte algae and diatoms (Rampen et al., 2012), but the C_{32} 1,15-diol is also produced by freshwater eustigmatophyte algae (Lattaud et al., 2021; Volkman et al., 1992). As a result, the abundance of the C_{32} 1,15-diol in continental margin sediments relative to marine diols has been proposed as proxy for freshwater discharge in marine systems (Lattaud et al., 2017). Finally, brGDGTs are membrane lipids synthesized by soil bacteria (Sinninghe Damsté et al., 2000) and used as a tracer for soil microbial OM (Hopmans et al., 2004). Although brGDGTs can also be produced in situ in coastal marine settings, the weighted number of internal cyclizations is higher in brGDGTs with a marine origin compared to those produced in soils and can thus be recognized as such (Dearing Crampton-Flood et al., 2019; Sinninghe Damsté, 2016). Hence, analysis of these biomarkers, together with total organic carbon (TOC), its stable carbon isotopic composition ($\delta^{13}C_{org}$), and mineral SA of different grain size fractions (≥250, 250–125, 125–63, 63–30, 30–10 and <10 μm) and bulk marine sediments along a land-sea transect (15–600 m water depth, Figure 1) away from the Atchafalaya River could lead to insights in the occurrence and role of organo-mineral associations on TerrOM dispersal patterns. Finally, X-ray diffraction (XRD) was used to assess mineral composition and thereby whether these biomarkers have an affinity for certain minerals.

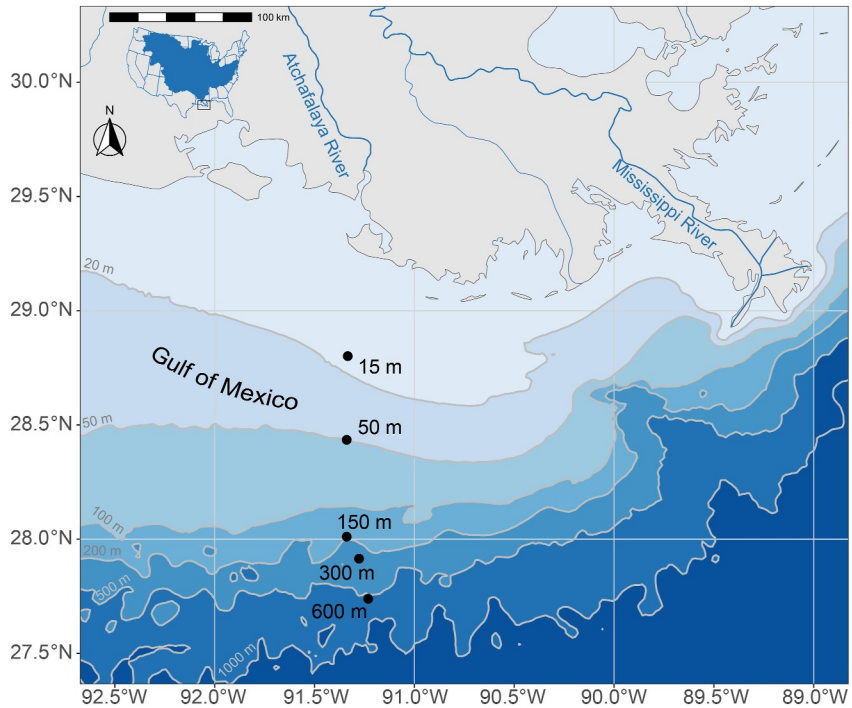

Figure 1. Sample locations along the Atchafalaya land sea transect in the northern Gulf of Mexico. The sediments were collected at 15, 50, 150, 300, and 600 m water depth.

2. Materials and Methods

2.1. Study Area and Sample Collection

With a combined annual water discharge of 22,800 $m^3\ s^{-1}$, the MAR represent the largest watershed of North America and form the main supplier of sediments, freshwater, and nutrients to the northern GoM (Meade & Moody, 2009; Neill & Allison, 2005). The outflow of the MAR is regulated by a control structure, which diverts 30% of the Mississippi stream flow toward the Atchafalaya River (Reuss, 2004). Sedimentation rates are highest (>10 cm y^{-1}) close to the Mississippi River mouth and decrease westward along the shelf (~1 cm y^{-1}, Corbett et al., 2006; Neill & Allison, 2005). The direction of the coastal currents in the northern GoM is mostly influenced by wind stress, driving the river discharge westward along the shelf (Walker et al., 2005). During summer months, a seasonal hypoxic zone forms in the northern GoM due to increased nutrient discharge from the MAR that trigger phytoplankton blooms on the Louisiana shelf (Rabalais et al., 2002).

Marine sediments were retrieved from a land-sea transect offshore the Atchafalaya River in March 2018 with the *R/V* Pelagia as part of the Netherlands initiative changing oceans (NICO) expedition. Sediments were collected from 5 locations at 15, 50, 150, 300, and 600 m water depth using a multicorer. Based on the bathymetry of the northern GoM (Figure 1), the 15 and 50 m water depth sites are located on the Louisiana shelf, whereas sediments at 150, 300, and 600 m water depth are located on the slope. We, therefore, refer to these two shallower sites as "coastal" and to the deeper sites as "offshore" in this manuscript. The multicores were sliced at 1 cm intervals and stored at −20°C until arrival in the laboratory, where they were freeze-dried. Sediment slices from the depth interval corresponding to the last ~15 years, based on available ^{210}Pb data (Lenstra et al., 2022), were combined and mixed for each site to enable direct comparison between sample locations. This corresponds to the integration of the upper 24, 22, 3, 2, and 4 cm of the sediments collected at 15, 50, 150, 300, and 600 m water depth, respectively. Although the coastal sites are located within the seasonal hypoxic zone, the 15-year integration method ensures that the targeted sediments also experienced oxic conditions, thereby removing potential preservation biases between the coastal and offshore sites. Geochemical data from Lenstra et al. (2022) furthermore show no evidence of prolonged hypoxic conditions in the top 15 cm at each site.

2.2. Grain Size Fractionation and Distribution

Freeze-dried sediments from each site were separated into six grain size fractions: <10, 10–30, 30–63, 63–125, 125–250, and ≥250 μm based on the Udden-Wentworth scale for sand and clay sizes (Wentworth, 1922). The fractions ≥63 μm were separated by wet sieving, while separation of the fractions <63 μm, where the mineral associated OM is primarily present (Kleber et al., 2021), was achieved by settling from suspension in graduated cylinders. To each suspension, 25 mL/L of a dispersant solution (44.6 g $Na_4P_2O_7 \cdot 10H_2O$ + 4.24 g Na_2CO_3/1 L H_2O) was added, mixed, and then allowed to settle. Upon settling of the targeted fraction, the supernatant containing the finer fraction(s) was removed by siphoning it into a clean graduated cylinder. Finally, the <2 μm fraction was separated from that <10 μm using centrifugation (Poppe et al., 1988; Svedberg & Nichols, 1923; Trask, 1930). The obtained fractions were rinsed with demineralized water to remove the dispersant and freeze-dried again. The grain size distribution of the bulk sediment was measured on a Malvern Mastersizer 2,000 (Malvern Instruments Limited) after the removal of carbonate and organics using 1M HCl and 6% peroxide, respectively.

2.3. Total Organic Carbon and Stable Carbon Isotope Analysis

For all grain size fractions and the bulk sediment, ~0.3 g of homogenized sediment was treated with 1 mL HCl overnight to remove carbonates and measured for TOC and $\delta^{13}C_{org}$ on a Thermo Scientific Flash Elemental Analyzer coupled to a Thermo Scientific Delta V Advantage isotope ratio mass spectrometer (IRMS). Total organic carbon is expressed as weight percentage (wt.%), and $\delta^{13}C_{org}$ values are reported in per mille relative to the Vienna Peedee belemnite standard (VPDB). Nicotinamide was used as lab standard and showed standard deviations of 0.049 for TOC and 0.03 for $\delta^{13}C_{org}$. Notably, the <30 μm size fractions from the site at 15 m water depth were awaiting further fractionation when the laboratories closed due to the covid pandemic and suffered from algal growth in the meantime. Therefore, these fractions are excluded from TOC and $\delta^{13}C_{org}$ analysis.

2.4. Mineral Surface Area

The mineral SA was obtained for 13 samples across size fractions and sampling locations that contained enough material for the analysis, mostly consisting of the <30 μm fractions, of which 0.5–1.5 g of freeze-dried material was combusted at 400°C for 12 hr to remove organic material and slowly cooled to avoid incomplete combustion. The combusted sediments were rinsed with demi-water and centrifuged to decant salts and ashes. Immediately prior to analysis, the sediments were degassed under vacuum (2 hr at 300°C) and then analyzed on a Nova 4200e SA Analyzer (Quantachrome Instruments) using a 6-point Brunauer-Emmett-Teller method (Brunauer et al., 1938). The measurements were compared with two reference materials (of 5.41 and 27.46 $m^2\ g^{-1}$, respectively) and showed an uncertainty of ~4%.

2.5. Lipid Biomarker Analysis and Proxies

Between 0.02 and 2.1 g of sediment was used for biomarker analysis depending on the size fraction. All sediment fractions were homogenized, and lipid biomarkers were extracted with 25 mL of dichloromethane (DCM): methanol 9:1 (v/v) using the Milestone Ethos X extraction system (MEX). The total lipid extract (TLE) was filtered over a sodium sulfate column and subsequently separated into apolar, neutral, and polar fractions by passing the TLE over a small column of activated aluminum oxide using hexane:DCM (9:1), hexane:DCM (1:1), and DCM:methanol (1:1) as the respective eluents.

The apolar fraction was analyzed on a gas chromatograph coupled to a flame ionization detector (GC-FID; Hewlett Packard 6890 series). The fractions were dissolved in hexane and co-injected with a known amount of squalene as standard. The GC-FID was equipped with a VF1 column (30 m × 0.32 mm, film thickness 0.10 μm) and operated at a constant pressure of 100 kPa using helium as carrier gas. The oven temperature program started at 70°C rising to 130°C at 20°C min^{-1} and then to 320°C at 4°C min^{-1}, which was held for 10 min.

A known amount of synthetic C_{46} GTGT standard was added to the polar fraction, which was then dissolved in hexane:isopropanol (99:1, v/v) and subsequently passed through a 0.45 μm polytetrafluorethylene filter. GDGTs were analyzed on a high performance liquid chromatography-mass spectrometer (HPLC-MS, Agilent 1,260 Infinity) with instrument settings according to Hopmans et al. (2016). In short, 10 μL of sample was injected after which the GDGTs were separated over two silica Waters UHPLC HEB Hilic Columns (1.7 μm,

2.1 mm × 150 mm) in tandem held at 30°C. GDGTs were eluted isocratically for 25 min at a flow rate of 0.2 mL min^{-1} using 82% hexane and 18% hexane:isopropanol 9:1 (v/v), followed by a linear gradient to 70% hexane and 30% hexane:isopropanol 9:1 (v/v) for 25 min. The GDGTs were ionized using atmospheric pressure chemical ionization, with a gas temperature of 200°C, vapourizer temperature of 400°C, N_2 flow of 6 L min^{-1}, capillary voltage of 3,500 V, nebulizer pressure of 25 psi, and a corona current of 5.0 µA. GDGT detection was performed by a single ion monitoring of the $[M + H]^+$-ions and quantified using Chemstation B.04.03 software.

An aliquot of the polar fraction was then silylated in pyridine with N,O-bis(trimethylsilyl)trifluoroacetamide (BSTFA) upon heating at 60°C for 20 min. The silylated polar fraction was dissolved in ethyl acetate and co-injected with an external squalene standard on the GC-FID following the same oven program as used for the analysis of apolar fractions. The polar fractions were subsequently injected on the gas chromatograph-mass spectrometer (GC-MS, Finnigan Trace GC Ultra) equipped with the same column and using the same oven program for peak identification and quantitative integration of the long-chain diols and the *n*-alcohols. The GC-MS operated at constant flow of 2.0 ml min^{-1} and the MS operated within a scanning range of *m/z* 50–800.

The average chain length (ACL) and the carbon preference index (CPI) of long-chain *n*-alkanes were calculated according to Marzi et al. (1993) and Poynter et al. (1989) to provide insight on the vegetation type and degradation state of the *n*-alkanes (Bray & Evans, 1961):

$$ACL = (25C_{25} + 27C_{27} + 29C_{29} + 31C_{31} + 33C_{33} + 35C_{35})/(C_{25} + C_{27} + C_{29} + C_{31} + C_{33} + C_{35}) \quad (1)$$

$$CPI = ((C_{23} + C_{25} + C_{27} + C_{29} + C_{31} + C_{33}) + (C_{25} + C_{27} + C_{29} + C_{31} + C_{33} + C_{35})) / (2 * (C_{24} + C_{26} + C_{28} + C_{30} + C_{32} + C_{34})) \quad (2)$$

The $\#rings_{tetra}$ quantifies the weighted number of cyclopentane rings in tetramethylated brGDGTs and can be used to identify in situ marine production of brGDGTs (Sinninghe Damsté, 2016):

$$\#rings_{tetra} = [(Ib) + 2\,(Ic)] / [(Ia) + (Ib) + (Ic)], \quad (3)$$

where roman numerals refer to molecular structure of brGDGTs.

2.6. X-Ray Diffraction Measurements

Bulk sediments were reduced to a fine powder and front-sideloaded onto PMMA sample holders with a cavity of 25 mm and analyzed on a Bruker D8 Advance X-ray diffractometer with a LYNXEYE detector and a θ/θ goniometer. A primary Soller slit of 2.5°, a variable divergence slit-resulting in a constant irradiated length of 20 mm, and a motorized anti-scatter screen were used. X-ray powder diffraction patterns were recorded from 3 to 80°2θ, in steps of 0.02°, counting for 0.85 s per step using Cu-*K*α radiation (40 kV, 40 mA). Samples were continuously spun (0.25 Hz) during measurement. To interpret the patterns thus obtained, the ICDD reference library of standard PXRD patterns of pure minerals was used.

Clay fractions (<2 µm) were analyzed on the composition of major clay groups, that is, chlorite, illite, kaolinite, and smectite. The <2 µm fraction at 15 m was excluded from analysis, as this fraction did not yield enough material. First, carbonate was removed from the <2 µm fractions using a 0.11 N HCl solution (see Ostrom, 1961). The reaction was allowed to take place for 1 hr at room temperature (20°C). After treatment with acid, the samples were rinsed three times with deionized water and freeze-dried. To saturate clay minerals with Mg, the suspensions were treated with a 0.1 M $MgCl_2$ solution. The suspensions were separated from the solution two times and, each time, the solution was replaced with fresh solution.

To prepare oriented clay mounts, the decalcified, $MgCl_2$-saturated <2 µm suspensions were vacuum-filtered through Millipore 0.45 µm membrane filters in a Millipore 47 mm glass filter kit for no longer than 10 min. The suspensions contained 147.2 mg of sediment in 45 mL of deionized water. This procedure (see Drever, 1973) helps ensure uniform and infinite sample thicknesses at 30°2θ on glass slides with an area of 625 mm^2 and using a slit width of 0.165 mm during measurement (Reynolds, 1989). The clay mounts were measured as described above using a primary Soller slit of 4.1°, and the samples were not spun during measurements. X-ray diffraction patterns were recorded from 3 to 33°2θ. Each sample was measured in three conditions: air-dried, after exposure

to the vapor of ethylene glycol in a dish with a lid for at least 8 hr in an oven at 60°C (see Bradley, 1945) and after having been baked at 550°C in a furnace for 6 hr. The major clay mineral groups were identified and quantified, and their weighted peak area percentages were estimated using the criteria of Biscaye (1965).

3. Results

3.1. Grain Size Distribution, TOC Content, and $\delta^{13}C_{org}$ of Grain Size Fractions

The bulk sediments were dominated by grain sizes <30 μm (45%–95% of the sediment) of which the contribution increases with water depth (Figure 2a). Coarser fractions (>250 and 125–250 μm) contributed <1% of the sediments at most sites. At 15 m water depth, the sediments were relatively evenly distributed over the grain sizes compared to further offshore. The TOC content of the bulk sediment varied between 0.5 and 0.8 wt.% and in the different size fractions between 0.1 and 2.6 wt.% (Figure 2b). In general, the TOC content was higher in the 125–250 μm fractions (average 1.3 wt.%, $n = 5$) compared with the finer fractions <30 μm (average 0.9 wt.%, $n = 8$). The range in TOC content in the different size fractions was more variable at sites ≤150 m water depth (0.1–2.6 wt.%, $n = 11$) than at those ≥300 m water depth (0.4–1.2 wt.%, $n = 12$). The $\delta^{13}C_{org}$ ranged from −21.6 to −23.1‰ (average −22.2‰, $n = 30$) and was most negative at the coastal sites (−21.8–−23.1‰) compared with the offshore sites (−21.6–−22.9‰, Figure 2c).

3.2. Mineral Surface Area of Grain Size Fractions

Mineral SA varied from 6.7 to 55.8 $m^2\ g^{-1}$ ($n = 13$, Figure 2d), where the finer grain size fractions (<30 μm) had a larger SA (24.3–55.8 $m^2\ g^{-1}$) compared with the coarser grain sizes (≥63 μm, <18.6 $m^2\ g^{-1}$). The SA of the grain sizes <30 μm, for which data is available for the whole transect, was lower close to the coast (water depth <50 m) compared with at sites >150 m water depth.

3.3. Biomarker Concentrations in Bulk Sediments and Grain Size Fractions

The long-chain *n*-alkanes ($C_{29–35}$), *n*-alcohols ($C_{22–28}$), C_{32} 1,15-diols, and brGDGTs were present in almost all size fractions except for the ≥250 μm fraction at 50 m water depth in which C_{32} 1,15-diols were not detected. Concentrations of bulk *n*-alkanes ranged from ~0.2–0.3 μg g^{-1} dry sediment (g_{dw}, Figure 3a). In the different grain size fractions, *n*-alkanes ranged from 0.03–1.43 μg g_{dw}^{-1} and decreased with increasing water depth. The *n*-alkane concentrations were generally high in both the coarsest (≥250 μm) as well as the finer (<30 μm) size fractions. Close to shore, the variation of *n*-alkane concentrations within different grain size fraction was larger than further offshore. When normalized to TOC, the *n*-alkane concentrations of bulk sediment and grain size fractions remained relatively stable along the transect (Figure 3b) except for a high TOC-normalized *n*-alkane concentration of 250 μg g^{-1} TOC in the 63–125 μm fraction at 15 m water depth. The *n*-alkane loadings reflect the relatively stable trend in the concentrations and ranged from 6.8–27.2 ng m^{-2}, where loadings were highest in the <30 μm fractions (Figure 3c). The ACL varied from 29.1 to 29.5 in the bulk sediments and 28.9 to 31.3 in the grain size fractions and was relatively similar except for the ≥250 μm fraction at 300 m water depth, where the ACL was much higher (Figure 3d). The CPI varied between 0.8 and 6.7 for both bulk sediment and different size fractions (Figure 3e). Generally, the CPI was >3 especially at 600 m water depth where the CPI ranged from 4 to 6.7.

Dry-weight concentrations of long-chain *n*-alcohols ranged from 0.2–0.7 μg g_{dw}^{-1} in the bulk sediments with the highest concentrations at 300 m water depth. In the grain size fractions, *n*-alcohol concentrations ranged from 0.03–1.16 μg g_{dw}^{-1} with the highest concentrations in the coarsest fraction at 15 m water depth (Figure 4a). Further along the transect, concentrations in the grain size fractions generally decreased and were <0.4 μg g_{dw}^{-1} at ≥150 m water depth. TOC-normalized *n*-alcohol concentrations of bulk sediments were highest at 15 m water depth and decreased further offshore with the exception of the sediments collected at 300 m water depth. In the grain size fractions, TOC-normalized concentrations decreased from 15 m water depth (60–125 μg g^{-1} TOC) toward 7–45 μg g^{-1} TOC in deeper ≥50 m waters (Figure 4b). The *n*-alcohol loadings decreased from 10–12 ng m^{-2} at 15 m water depth toward <2 ng m^{-2} at 600 m water depth (Figure 4c).

The concentrations of C_{32} 1,15-diols were low in both bulk sediments (0.005–0.02 μg g_{dw}^{-1}) and grain size fractions (0–0.06 μg g_{dw}^{-1}) and decreased further offshore (Figure 5a). At the coastal sites, C_{32} 1,15-diol concentrations were highest in size fractions ≥125 μm (0.06 μg g_{dw}^{-1}). Only at 300 m water depth, C_{32} 1,15-diols

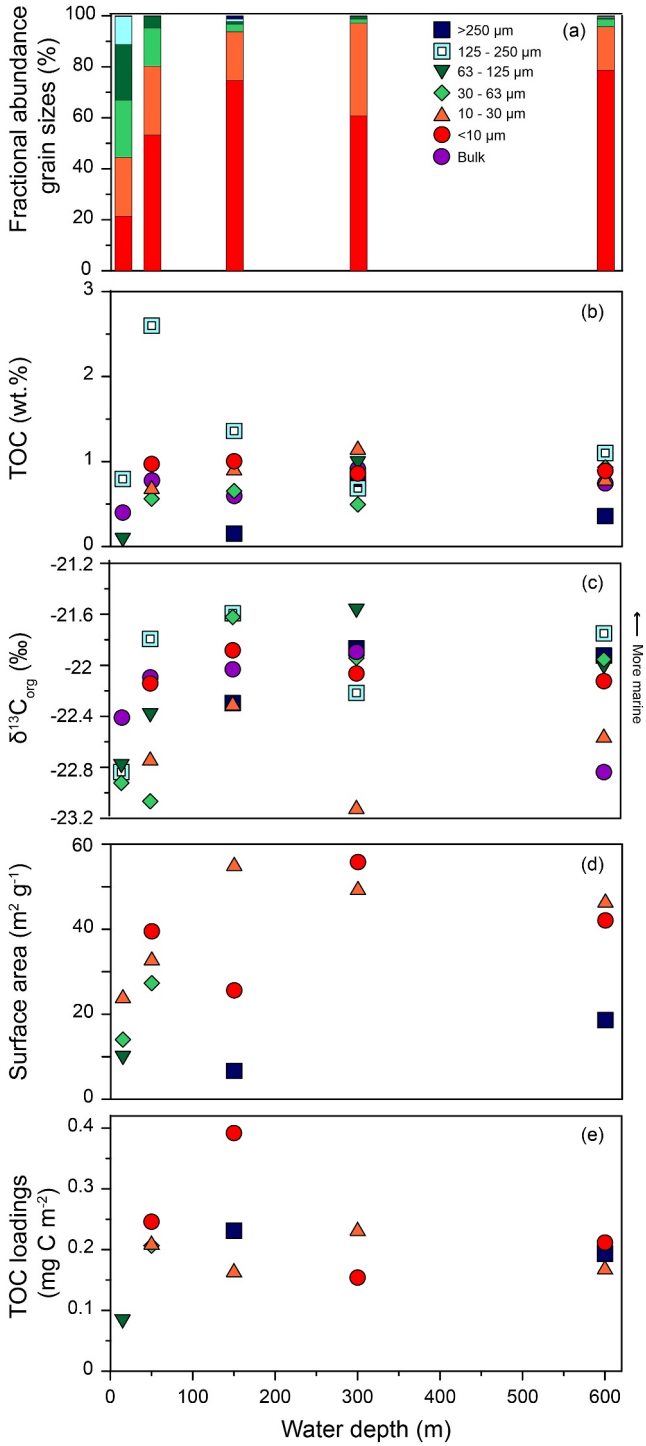

Figure 2. (a) Grain size distribution (b) total organic carbon (TOC) content, (c) $\delta^{13}C_{org}$ values, (d) mineral surface area (SA), and (e) TOC/SA loadings in bulk sediment and different grain size fractions along the Atchafalaya land-sea transect. In some grain size fractions, the relative contribution was <1%. Grain size fractions are represented with different colors and symbols.

were most abundant in small size fractions (<10 µm). TOC-normalized C_{32} 1,15-diol concentrations of the bulk sediment decreased from 15 to 50 m water depth and remained low further offshore (3.8–0.7 µg g^{-1} TOC from 15–600 m, Figure 5b). Within the grain size fractions, the C_{32} 1,15-diol concentrations also decreased further offshore except for the ≥250 µm fraction at 300 and 600 m and the <10 µm fraction at 300 m water depth (Figure 5b). The C_{32} 1,15-diol loading decreased rapidly offshore from 0.73–0.19 ng m^{-2} from 15 to 600 m water depth (Figure 5c). Overall, high C_{32} 1,15-diol loadings were found in the 10–30 µm fraction at 15m and in the ≥250 µm fraction at 600 m water depth, where loadings in the <30 µm fraction were low.

BrGDGT concentrations of bulk sediments ranged from 0.04 to 0.15 µg g_{dw}^{-1} and were highest at 50 m water depth (Figure 6a). In the grain size fractions, brGDGT concentrations ranged from 0.01 to 0.26 µg g_{dw}^{-1} and were generally highest in the fine (<10 µm) grain size fraction. Concentrations in all fractions decreased rapidly from 15 to 600 m water depth (average 0.12–0.04 µg g_{dw}^{-1}) also after normalizing to TOC (26–5 µg g^{-1} TOC from 15 to 600 m, Figure 6b) and SA (4.4–1.2 ng m^{-2}, ~73% decrease from 15 to 600 m water depth, Figure 6c). The loadings were highest in the fine (<30 µm) fractions. In the bulk sediments, TOC-normalized brGDGT concentrations were high in the coastal sites and decreased further offshore. The $\#rings_{tetra}$ increased from 15 to 150 m water depth (0.5–0.7 to 0.5–0.9) in both the bulk sediments and grain size fractions (Figure 6d). High values were found at 50 m (0.7–0.8) and 150 m water depth (0.5–0.9). Further offshore, the $\#rings_{tetra}$ values decreased to 0.4–0.6 with little variation between grain size fractions.

3.4. Mineral Composition of Clay Fractions

The XRD diffraction patterns derived from the clay fractions (<2 µm) indicate that the mineral composition was similar at all sites, whereby smectite was the most abundant mineral (50%–56%) followed by illite (25%–28%) and kaolinite (18%–22%). Chlorite was not detected.

4. Discussion

4.1. TOC in Relation to Grain Size and Mineral Surface Area

The grain size distribution of the bulk sediments indicates that most of the sediment is ≤30 µm especially further offshore (Figure 2a). The TOC content is generally high in these fractions, although the highest TOC is found in the 125–250 µm fractions at most sites (Figure 2b). Although this fraction does not substantially contribute to the total sediment (11% at 15 m and <1% at ≥50 m), this contrasts earlier studies that find the highest TOC contents in the fine grain size or low-density fractions in shelf environments, including the Louisiana shelf (Bergamaschi et al., 1997; Hou et al., 2020; Kusch et al., 2019; Mayer, 1994a, 1994b). Possibly, the TOC in these coarser fractions is not solely associated to mineral surfaces but also as discrete (plant) material as has also been suggested earlier (Galy et al., 2011; Keil et al., 1994b). However, 125–250 µm fractions with the high TOC content generally also have high $\delta^{13}C_{org}$ values. Although this may indicate that the TOC is derived from C4 plants, it can also point toward a marine contribution (Figures 2b and 2c). Nevertheless, this grain size fraction only represent a small fraction of the bulk sediment. To assess whether OC is associated to mineral surfaces, TOC is normalized to mineral SA for the different grain size fractions (Figure 2e). The loading of TOC on mineral surfaces (i.e., OC/

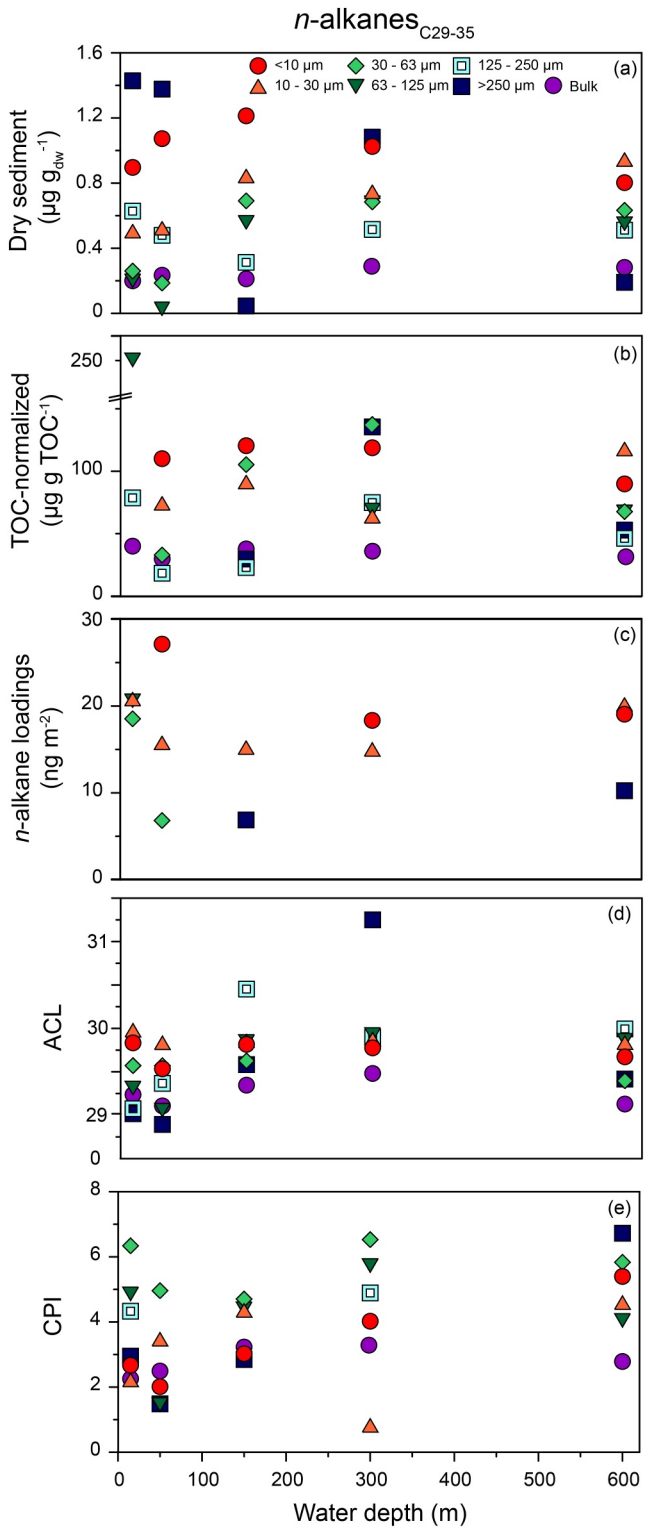

Figure 3. Concentrations and loadings of long-chain *n*-alkanes in bulk sediment and different grain size fractions along the Atchafalaya land-sea transect. The *n*-alkane concentrations are normalized against (a) dry sediment, (b) total organic carbon, and (c) mineral surface area. (d) average chain length and (e) carbon preference index are also shown. Grain size fractions are represented with different colors and symbols.

SA) is <0.4 mg OC m^{-2} for all size fractions along the transect, where the smallest size fractions (<10 and 10–30 µm) have the highest loadings (Figure 2e). The range of OC/SA is representative of a deltaic system with high sediment input, such as the Louisiana shelf (Figure 7; Blair & Aller, 2012; Mayer, 1994b) and also within previously published OC/SA values for bulk sediments from the Mississippi river and northern GoM slope and shelf sediments (0.2–0.4 mg OC m^{-2}; Gordon & Goñi, 2003; Mayer, 1994b; Waterson & Canuel, 2008; Wakeham et al., 2009). The general positive relationship between TOC and SA in our data thus suggests that OC is indeed protected by mineral surfaces.

The $\delta^{13}C_{org}$ is lowest close to shore at 15 m water depth and becomes less negative in deeper waters, consistent with a change from more terrestrial to more marine OM (Hedges et al., 1997). This trend is consistent with previous studies in the northern GoM (Gordon & Goñi, 2003; Wakeham et al., 2009; Yedema et al., 2023) and particularly clear in fractions ≥30 µm. The $\delta^{13}C_{org}$ in the finer fractions (<30 µm) remains low with increasing water depth, suggesting that TerrOM is mostly associated with minerals in these fractions, or that bonds between OM and mineral surfaces are best maintained in the marine environment. Notably, previous studies suggested that plant material derived from C4 grasslands in the upper Mississippi basin could be preferentially transferred offshore due to mineral protection and hydrodynamic sorting (Bianchi et al., 2011; Goñi et al., 1997; Ware et al., 2022). This pool of TerrOM is often overlooked due to its $\delta^{13}C_{org}$ signature that is similar to that of marine OM. Hence, we cannot exclude the presence of C4 plant material in deeper waters based on the $\delta^{13}C_{org}$.

4.2. Evolution of Biomarker Concentrations and Loadings Along the Atchafalaya Transect

4.2.1. Long-Chain *n*-Alkanes

Long chain *n*-alkanes, derived from leaf waxes of vascular plants, represent a constant fraction of the TOC along the land-sea transect (Figure 3). Only their abundance in the ≥250 µm fraction varies substantially with water depth, although this fraction contributes little to the total sediment. Nevertheless, it suggests that varying contributions of plant detritus that is not associated to mineral surfaces is present along the transect. Previous studies have indicated that discrete plant particles can account for up to 95% of all OM in coarse grain size fractions in both rivers and coastal marine environments (Bergamaschi et al., 1997; Dickens et al., 2006; Keil et al., 1994b; Repasch et al., 2022). The fluctuating concentrations of *n*-alkanes in the coarse fractions furthermore indicate that discrete particles are unevenly distributed in the coastal zone. In contrast, *n*-alkane concentrations in the bulk sediments, which can be considered more homogenized and representative, remain relatively stable along the transect. This trend holds when the *n*-alkane concentration in the size fractions are normalized to mineral SA, suggesting that *n*-alkanes are indeed protected by mineral surfaces in the marine realm. The *n*-alkane loadings are generally highest in the <10 µm and 10–30 µm fractions, which imply that they are most likely bound to silt and clay minerals, as has also been found in soils, rivers, and other coastal environments (e.g., Bergamaschi et al., 1997; Feng et al., 2005; Freymond et al., 2018; Mikutta et al., 2009; Quenea et al., 2004; Repasch et al., 2022; van der Voort et al., 2017; Wakeham et al., 2009). The consistent contributions of *n*-alkanes to TOC and their loading on mineral surfaces suggest that their associations with clay and silt minerals hold during fluvial transport as well as after discharge to the marine realm. Notably, these

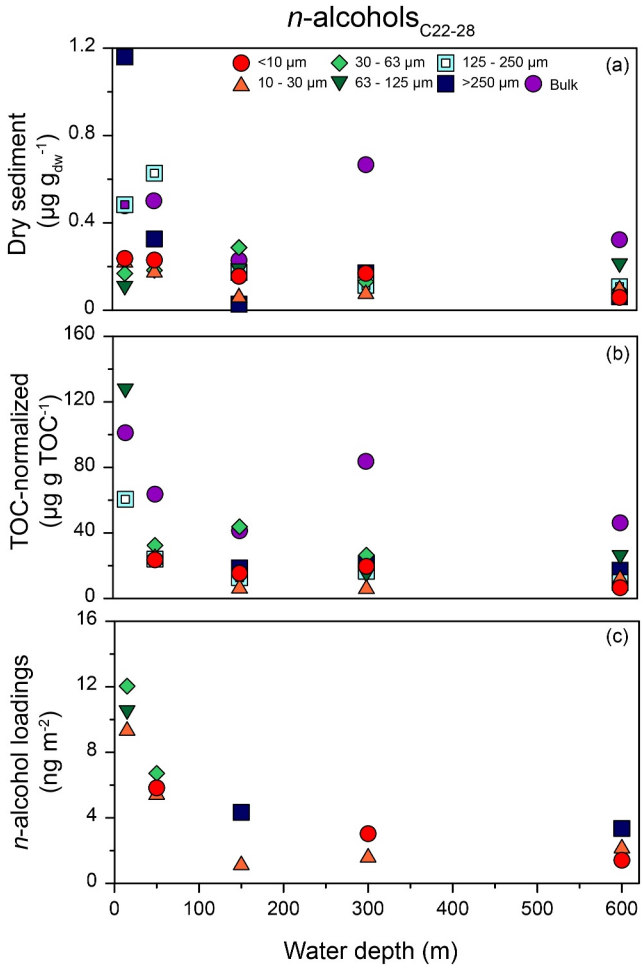

Figure 4. Concentrations and loadings of long-chain *n*-alcohols in bulk sediment and different grain size fractions along the Atchafalaya land-sea transect. The *n*-alcohol concentrations are normalized against (a) dry sediment, (b) total organic carbon, and (c) mineral surface area. Grain size fractions are represented with different colors and symbols.

associations make them susceptible to hydrodynamical sorting, where fine-grained material is preferentially transported further offshore. Previous studies have found that *n*-alkanes can indeed be transported further offshore compared with other plant-derived biomarkers (e.g., long-chain fatty acids, lignin, and cutin) along land-sea transects in the Laptev Sea, South China Sea, and the East Siberian Sea (Bröder et al., 2016, 2018; Hou et al., 2020; Jong et al., 2023; Tesi et al., 2014, 2016). Although this trend can be linked to mineral protection, *n*-alkanes are also more recalcitrant than most other plant molecules, potentially contributing to their preferential preservation and transport offshore (Bröder et al., 2016; Hoefs et al., 2002; Tesi et al., 2014). However, the ACL does not show any clear trend along the transect, arguing against the preferential transport of certain chain lengths (Figure 3d). In addition, the lack of a clear trend in ACL suggests that the source of long-chain *n*-alkanes remains relatively constant along the transect, whereas preferential offshore transport of C4 grassland material derived from the upper Mississippi basin would have resulted in a trend toward higher ACL. Nevertheless, relatively high ACL values in the 125–250 µm fraction correspond well to high $\delta^{13}C_{org}$ values and could indicate a higher presence of C4 material in this fraction, although the presence of diatom opal frustules in coarse grain size fractions in this area could similarly suggest that the OM in this fraction is of marine origin rather than comprised of C4 plant material (Lattaud et al., 2022). Furthermore, the CPI on *n*-alkanes in the grain size fractions is generally between 3 and 6 and does not decrease further offshore (Figure 3e), which suggests that *n*-alkanes are not degraded during transport and are thus likely associated to mineral surfaces. Finally, aeolian transport could also contribute to the offshore dispersal of *n*-alkanes, the MAR is assumed to be the main supplier of *n*-alkanes to the northern GoM (Kusch et al., 2021; Suh et al., 2019).

4.2.2. Long-Chain *n*-Alcohols

Both the concentrations and loadings of long-chain *n*-alcohols, derived from terrestrial plants, decrease rapidly after 15 m water depth along the Atchafalaya transect. This offshore pattern is very dissimilar from the trend in *n*-alkanes (Figures 3 and 4), despite their shared plant-derived source. Furthermore, the *n*-alcohol concentrations vary less between grain sizes compared with the n-alkanes. Since both *n*-alkanes and *n*-alcohols are considered to be resistant to degradation (Hoefs et al., 2002; Lützow et al., 2006), the dissimilar behavior between these two higher plant biomarkers along the transect suggests that the association between *n*-alcohols and mineral surfaces is weaker than that of *n*-alkanes. This can be the result of the hydroxyl-group that characterizes *n*-alcohols, which can influence the type of bond of this biomarker with mineral surfaces (Keil & Mayer, 2014). However, previous studies that compared offshore trends in *n*-alkanes to other plant markers, including *n*-alcohols, report less pronounced differences than shown in this study (e.g., Bröder et al., 2018; Hoefs et al., 2002; Hou et al., 2020). Although long-chain (>C_{22}) *n*-alcohols are generally attributed to higher plants (e.g., Treignier et al., 2006; Hemingway et al., 2016), C_{22}–C_{28} *n*-alcohols (especially C_{24}) have also been detected in eustigmatophyte algae in freshwater environments (Volkman et al., 1999), which are also the likely producer of the C_{32} 1,15-diols. Along the Atchafalaya transect, the C_{24} *n*-alcohol (dry weight concentration) correlate much better with the C_{32} 1,15-diols ($r = 0.8$, $p < 0.05$) than with the *n*-alkanes ($r = 0.3$, $p < 0.05$). This suggests that the *n*-alcohols might also have a different source than the *n*-alkanes along the Atchafalaya transect, which could explain their dissimilar dispersal in the marine realm. Another possibility for the different distributions of *n*-alkanes and *n*-alcohols could be a difference in their chemical structure. For instance, *n*-alcohols contain a hydroxyl group, which has the ability to form different bonds with mineral surfaces compared with *n*-alkanes. These bonds might be preferentially broken down in aquatic environments.

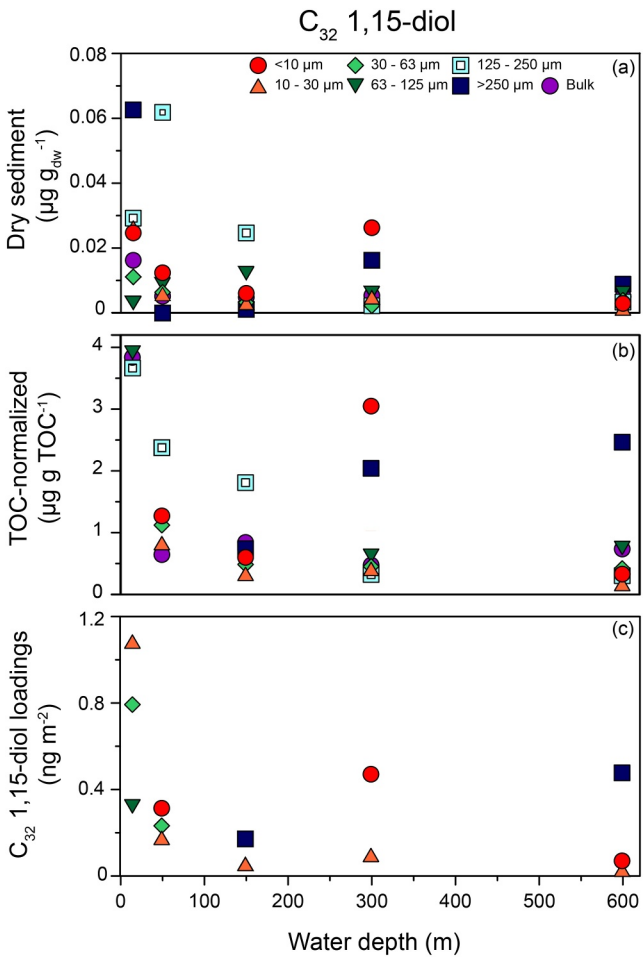

Figure 5. Concentrations and loadings of C_{32} 1,15-diols in bulk sediment and different grain size fractions along the Atchafalaya land-sea transect. The C_{32} 1,15-diol concentrations are normalized against (a) dry sediment, (b) total organic carbon, and (c) mineral surface area. Grain size fractions are represented with different colors and symbols.

4.2.3. C_{32} 1,15 Diols

Similar to the *n*-alcohols, the concentrations and loadings of C_{32} 1,15-diols, produced by freshwater algae, decrease rapidly after 15 m water depth and remain low in deeper waters (Figure 5). This indicates that C_{32} 1,15-diols are not transported far offshore. This trend is less pronounced in the TOC-normalized concentrations, where C_{32} 1,15-diols are more abundant in the <10 µm fraction at 300 m and >250 µm size fractions at 300 and 600 m water depth than at 50–150 m water depth. As the <10 µm fraction represents 60% of the bulk sediment at 300 m, the high concentrations of the C_{32} 1,15-diol could indicate a contribution of in situ produced C_{32} 1,15-diols, as has been shown to occur in the South China Sea based on similar distribution patterns of the C_{32} 1,15-diols and that of C_{30} 1,15-diols and other marine biomarkers (Yu et al., 2018). Although this pattern was also observed for the northern GoM (Yedema et al., 2023), they found that in situ production of C_{32} 1,15-diols likely occurred closer to the coast. In addition, the hydrogen isotopic composition of C_{32} 1,15-diols in sediments along this transect suggests that the majority of the diols has a freshwater origin (Lattaud et al., 2019). Hence, marine production cannot explain their higher concentrations at water depths >300 m. Additionally, hydrodynamic sorting seems unrealistic given the rapidly decreasing loadings of C_{32} 1,15-diols on mineral surfaces (Figure 5).

In contrast to *n*-alkanes, which can form associations with mineral surfaces in soils, C_{32} 1,15-diols are produced in the water column of stagnant parts of rivers and lakes (Shimokawara et al., 2010). These minerals are less readily available and may thus possibly limit the formation of associations with mineral surfaces. Alternatively, the role of C_{32} 1,15-diols as building blocks of the aliphatic biopolymer algaenan, which is a component of the outer wall of freshwater eustigmatophytes, has also been detected in some marine algae (Gelin et al., 1996; Largeau et al., 1986; Volkman et al., 1999) may be of importance here. Algaenan is highly hydrophobic and chemically resistant against degradation and releases ether-linked long-chain diols during prolonged oxygen exposure (Reiche et al., 2018), providing a mechanism for the transportation and preservation of the C_{32} 1,15-diols along the transect rather than the formation of associations with mineral surfaces. This alternative transport mechanism would also imply that C_{32} 1,15-diols are less susceptibility to hydrodynamic sorting, which is also evident from their weak correlation to grain size observed here as well as the absence of a correlation to bulk organic carbon content reported earlier (Lattaud et al., 2022). Overall, the decrease in loadings further offshore, combined with a low sensitivity to hydrodynamical sorting, suggests that C_{32} 1,15-diols are not associated to mineral surfaces in the GoM.

4.2.4. BrGDGTs

The concentrations and loadings of brGDGTs, primarily produced by soil bacteria, decrease rapidly after discharge and make up an increasingly smaller part of the TOC with increasing water depth, indicating that soil-derived brGDGTs are not transported far offshore (Figure 6). The rapid decrease in brGDGT concentrations toward the offshore sites is similar to the offshore trends in *n*-alcohols and C_{32} 1,15-diol concentrations. The decrease in brGDGT concentrations and loadings suggests that if brGDGTs were associated to mineral surfaces prior to discharge, they are rapidly released upon entering the marine realm, as has also been found in other river systems where the offshore dispersal of brGDGTs appears to be limited to the proximity of the river mouth (Sinninghe Damsté, 2016; Yedema et al., 2023; Zell et al., 2014a, 2014b). Earlier studies on brGDGT transport in rivers and coastal zones suggest that brGDGTs are only weakly linked to mineral surfaces based on, for example, the more rapid decrease of brGDGT loadings with increasing transport distance compared with the loadings of higher plant-derived fatty acids and lignin phenols in the Danube River (Freymond et al., 2018). In the Madre de Dios and Godavari River watersheds, stable brGDGT distributions in river depth profiles and riverbed sediment grain size fractions led to the conclusion that brGDGTs are not transported as organo-mineral moieties but might

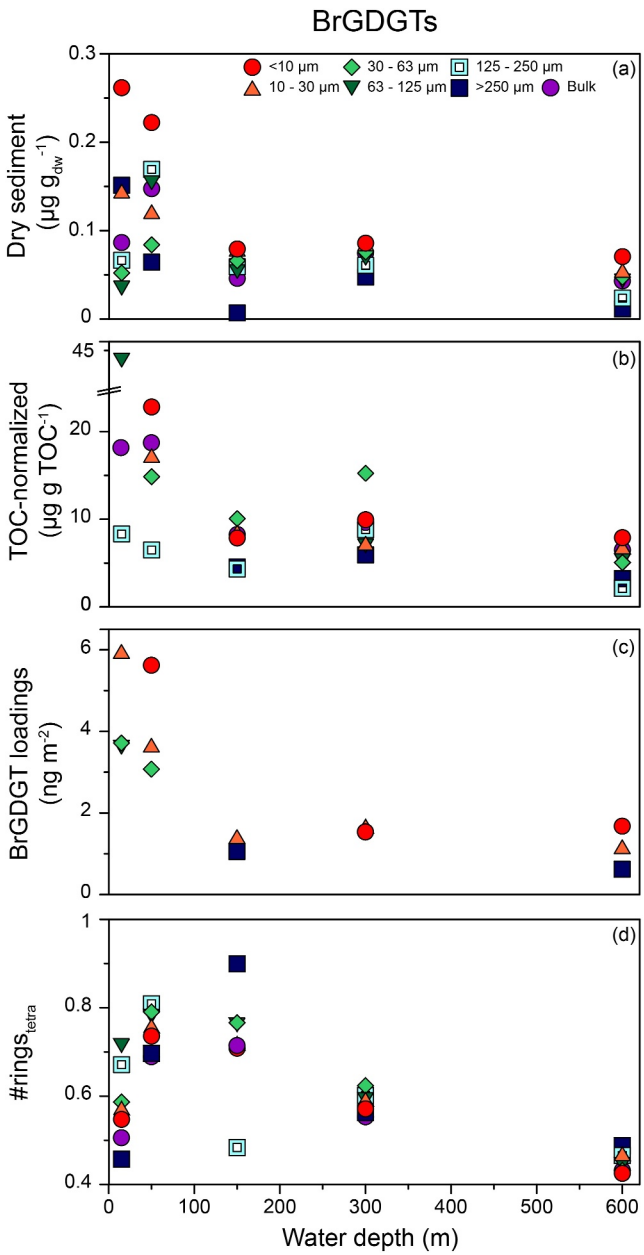

Figure 6. Concentrations and loadings of branched glycerol dialkyl glycerol tetraethers (brGDGTs) in bulk sediment and different grain size fractions along the Atchafalaya land-sea transect. The brGDGT concentrations are normalized against (a) dry sediment, (b) total organic carbon, and (c) mineral surface area. (d) The #rings$_{tetra}$. Grain size fractions are represented with different colors and symbols.

form colloids instead (Kirkels et al., 2020, 2022). Along the Atchafalaya transect, brGDGTs also appear to be evenly loaded on mineral surfaces among the different grain size fractions especially in deeper waters. The lack of selective association of brGDGTs with a specific size fraction was also seen in the Changjiang Estuary (Wang et al., 2024) and suggests that brGDGTs are not or less tightly bound to mineral surfaces compared with plant biomarkers and are, therefore, not impacted by hydrodynamical sorting processes.

Moreover, brGDGTs are also produced in coastal marine environments, specifically between 50 and 300 m water depth (Sinninghe Damsté, 2016), which would add to the brGDGT concentration of the sediment in this zone. This could explain the higher brGDGT concentrations in the bulk sediments at 50 m compared with 15 m water depth. A contribution of in situ produced brGDGTs can be recognized by high #rings$_{tetra}$ values (>0.7, Sinninghe Damsté, 2016). Indeed, high values for #rings$_{tetra}$ in the size fractions from 50 to 150 m water depth indicate that the largest part of the brGDGT pool in these sediments has a marine origin (Figure 6d). This implies that the loss of soil-derived brGDGTs is even larger than can be inferred from brGDGT concentrations. The #rings$_{tetra}$ further fluctuates per grain size in shallower (≤150 m water depth) sites (0.46–0.9) but not at 300 and 600 m water depth, where it remains stable among grain size fractions (0.57–0.62 and 0.43–0.49, respectively) similar to the brGDGT concentrations. This lack of selective association of brGDGTs with a specific size fraction further suggests that terrestrially derived brGDGTs are most likely not transported as organo-mineral associated OM.

4.3. Influence of Mineralogy on Biomarker Loadings

Next to OM type, mineralogy can also have an influence on the strength of associations with OM in relation to their interlayer structure. Smectite is the dominant clay mineral in the GoM (≥50%, see also Sionneau et al., 2008; Ito & Wagai, 2017) followed by illite and kaolinite. These phyllosilicates are all characterized by extensive interlayer space, which results in a high mineral SA that can accommodate OM (e.g., Feng et al., 2005; Ransom et al., 1998). The structure of illite and smectite minerals in particular facilitates the formation of associations with organic matter (Carroll, 1959; Ransom et al., 1998; Saidy et al., 2013; Wei et al., 2021). However, TerrOM seems to be systematically stripped from smectite surfaces upon discharge compared with from illite and kaolinite minerals (Blattmann et al., 2019). This has been attributed to the likely delamination of smectite particles with increasing salinity, whereby Ca ions are interchanged with Na ions (Brockamp, 2011). Previous studies also found that aliphatic compounds, such as the biomarkers targeted here, have a higher affinity for kaolinite surfaces in soils, whereas smectite clays generally complex with aromatic compounds (Feng et al., 2005; Wattel-Koekkoek et al., 2001). Hence, a differentiation in mineral protection and thus susceptibility to hydrodynamic sorting may occur if, in this case, *n*-alkanes are associated to different clay minerals than *n*-alcohols, long-chain diols, and brGDGTs. For example, the low abundances of *n*-alcohols, brGDGTs, and long-chain diols in offshore sediments of the GoM could result from their initial affinity with smectite minerals, which were stripped of their TerrOM content upon discharge. This could suggest that TerrOM is less well-preserved in continental shelf environments where smectite is the dominant clay mineral (see Zhao et al., 2023 for a global distribution of smectite in marine sediments). For example, high smectite content is found in the Godavari River basin (65%, Usman et al., 2018), where brGDGTs are indeed scarce in offshore sediments (Kirkels et al., 2022), although plant waxes are still present (Ponton et al., 2012). In contrast, smectite content is low offshore the Congo River (~10% close to shore,

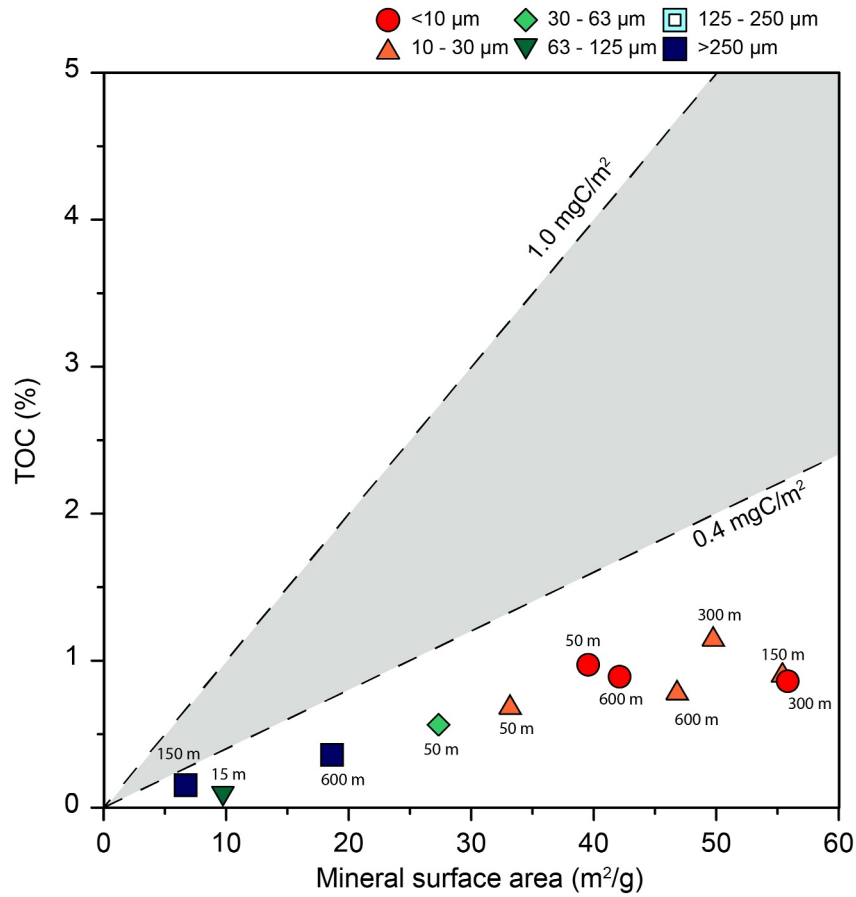

Figure 7. Total organic carbon versus mineral surface area for size fractions of sediments in the northern Gulf of Mexico. The gray area represents the range of 0.4–1 mg C m^{-2} common for shelf sediments according to Mayer (1994b). Here, values of >1 mg C m^{-2} are generally found in high productivity or low oxygen regions, whereas values of <0.4 mg C m^{-2} are typical for deltaic areas receiving large sediment inputs. Grain size fractions are represented with different colors and symbols.

Dinis et al. (2020)), where both brGDGTs and plant waxes are well-preserved (Weijers et al., 2009). Similar results are also found in the East China Sea, which has a low smectite content (Liu et al., 2014) and the offshore presence of soil-derived brGDGTs (Wang et al., 2024). Nevertheless, this trend between smectite and TerrOM content is not yet fully explored in the literature and therefore remains speculative.

Another option for the observed differences in biomarker loadings is *n*-alkanes would form organo-mineral associations while *n*-alcohols, long-chain diols, and brGDGTs are seemingly not associated with mineral surfaces in aquatic environments. As discussed above, long-chain diols might be transported as part of the biopolymer algaenan, whereas for brGDGTs, their distinct hydrophobic nature possibly inhibits them from moving to a dissolved phase and they form colloids instead after which they either degrade or stay dispersed in the water column (e.g., Kirkels et al., 2022; Yedema et al., 2023). Nonetheless, *n*-alkanes are also hydrophobic compounds, which raise the question why these compounds would be better associated with mineral surfaces compared with the *n*-alcohols, long-chain diols, and brGDGTs. Notably, the latter three biomarkers do all have a hydroxyl group in their chemical structure in contrast to the *n*-alkanes. As mentioned in the discussion on the *n*-alcohols, the presence of this functional group possibly results in a different bond with mineral surfaces that is more easily broken down in the marine realm. Moreover, a vast array of processes occur at the organo-mineral interface, including the transfer of electrons and the production of reactive oxygen species, which could in turn oxidize OM (Dong et al., 2023; Kleber et al., 2021). Perhaps, the presence of reactive groups in *n*-alcohols, diols, and brGDGTs compared with *n*-alkanes could further selectively deoxidize these groups, resulting in the prevalence of *n*-alkanes as compared with the other biomarkers. The use of chemical dispersant during the fractionation of the <63 µm size fractions could possibly replace sorbed OM as well (Castellini et al., 2013). This process could result

in lower TOC values and in extent lower OC/SA values for the northern GoM but could also cause differences in biomarker trends if specific OM groups would be replaced by the dispersant. However, the biomarker ratios mentioned here (e.g., ACL, CPI, and $\#rings_{tetra}$) for the different grain size fractions compare well to the bulk sediments and surface sediment data set of Yedema et al. (2023), indicating that if the dispersant replaced OM from mineral surfaces, this process was nonselective and therefore likely had little influence on the observed trends in biomarker concentrations.

Lastly, another possibility could be that the transport of hydrophobic OM in the marine realm, which includes the biomarkers studied here, is not facilitated by organo-mineral associations, which questions the general consensus that the majority of TerrOM in marine sediments is associated to mineral surfaces (Hedges & Keil, 1995; Kennedy & Wagner, 2011). For instance, Wei et al. (2021) studied the associations of algal OM, consisting of hydrophilic, hydrophobic, and humic acid-like substances, to different clay minerals in lake sediments. Their study showed that relatively large amounts of hydrophilic components were affiliated to clay surfaces, whereas hydrophobic substances were scarcely adsorbed. This phenomenon likely arises in response to the nature of the bonds between OM and mineral surfaces; Although hydrophobic compounds generally form weak Van der Waals bonds with minerals, hydrophilic adsorption occurs via stronger hydrogen bonding, augmenting the organo-mineral association (Chen & Diao, 2011; Karatapanis et al., 2011). Possibly, the biomarkers used in this study also form the weaker Van der Waals bonds, which are subsequently broken during the transition from soils to a fresh water or marine environment. The resulting land-sea trends observed in our biomarkers along the Atchafalaya transect might then rather represent a degradation signal instead of a decrease in mineral loadings, as *n*-alkanes are more resistant against degradation compared with *n*-alcohols, long-chain diols, and brGDGTs (e.g., Hoefs et al., 2002). These trends were also seen previously in the northern GoM, where *n*-alkanes were transported further offshore than C_{32} 1,15-diols and brGDGTs (Yedema et al., 2023). In any case, since the mineralogy remains stable along the transect, variations in loading trends among the different biomarkers along the Atchafalaya land-sea transect are likely more dependent on the type of the TerrOM than on the (clay) mineralogy.

5. Conclusions

To investigate the different dispersal patterns of plant, fluvial, and soil-microbial OM along a land-sea transect in the northern GoM, dry weight and TOC-normalized concentrations of *n*-alkanes, *n*-alcohols, C_{32} 1,15-diols, and brGDGTs were compared with their biomolecular loadings for different grain size fractions. The TOC loading on mineral surfaces (OC/SA) along the transect was typical for deltaic regions with high sedimentation rates, where fine size fractions with high SA had the highest TOC loadings. Biomarkers concentrations were generally highest in the fine size fractions except close to shore, where discrete plant particles likely contributed to the TOC content of the coarse fractions. Biomarker concentrations and loadings showed that *n*-alkanes remained most constant with increasing water depth, whereas *n*-alcohols, C_{32} 1,15-diols, and brGDGTs rapidly decreased further offshore. This indicates that the transport of *n*-alkanes is likely facilitated by organo-mineral associations of clay minerals and is susceptible to hydrodynamic sorting, whereas the other biomarkers are likely lost from mineral surfaces after discharge or possibly transported as part of the algaenan or as colloids prior to degradation. However, this trend could also occur due to a higher resistance to degradation of *n*-alkanes compared with the other biomarkers. Furthermore, the stable mineralogy along the transect indicates that the TerrOM type is the primary control on the persistence and subsequent transport of organo-mineral associations in the marine realm, although that the delamination of smectite, the dominant clay mineral in the GoM, can possibly contribute to the loss of TerrOM after discharge. Together, our data shows that different affinities of TerrOM biomarkers to form associations with mineral surfaces can explain the differential dispersal of plant, fluvial, and soil-microbial OM in the northern GoM, but that resistance against degradation possibly plays a role in smectite-rich environments.

Conflict of Interest

The authors declare no conflicts of interest relevant to this study.

Data Availability Statement

The data set supporting this study is accessible at Zenodo (https://doi.org/10.5281/zenodo.10939975).

Acknowledgments
The authors thank the editor and three anonymous reviewers whose feedback. We also thank Desmond Eefting, Arnold van Dijk, Anita van Leeuwen-Tolboom, Daisy Bouwmans, Dirk Jong, Coen Mulder, and Wesley Plugge for their laboratory assistance. This research was financially supported by the NESSC Gravitation Grant (024.002.001) from the Dutch Ministry of Education, Culture and Science (OCW). We acknowledge the funding of the Netherlands Organization for Scientific Research NWO and the Royal Netherlands Institute for Sea Research in organizing the Netherlands Initiative Changing Oceans NICO expedition in 2018 and in particular the captain and crew of the *R/V* Pelagia during leg 7 (64PE434).

References

Angst, G., Mueller, K. E., Kögel-Knabner, I., Freeman, K. H., & Mueller, C. W. (2017). Aggregation controls the stability of lignin and lipids in clay-sized particulate and mineral associated organic matter. *Biogeochemistry*, *132*(3), 307–324. https://doi.org/10.1007/s10533-017-0304-2

Angst, G., Mueller, K. E., Nierop, K. G., & Simpson, M. J. (2021). Plant-or microbial-derived? A review on the molecular composition of stabilized soil organic matter. *Soil Biology and Biochemistry*, *156*, 108189. https://doi.org/10.1016/j.soilbio.2021.108189

Bergamaschi, B. A., Tsamakis, E., Keil, R. G., Eglinton, T. I., Montluçon, D. B., & Hedges, J. I. (1997). The effect of grain size and surface area on organic matter, lignin and carbohydrate concentration, and molecular compositions in Peru Margin sediments. *Geochimica et Cosmochimica Acta*, *61*(6), 1247–1260. https://doi.org/10.1016/S0016-7037(96)00394-8

Berner, R. A. (1982). Burial of organic carbon and pyrite sulfur in the modern ocean: Its geochemical and environmental significance. *American Journal of Science*, *282*(4), 451–473. https://doi.org/10.2475/ajs.282.4.451

Bianchi, T. S., Cui, X., Blair, N. E., Burdige, D. J., Eglinton, T. I., & Galy, V. (2018). Centers of organic carbon burial and oxidation at the land-ocean interface. *Organic Geochemistry*, *115*, 138–155. https://doi.org/10.1016/j.orggeochem.2017.09.008

Bianchi, T. S., Wysocki, L. A., Schreiner, K. M., Filley, T. R., Corbett, D. R., & Kolker, A. S. (2011). Sources of terrestrial organic carbon in the Mississippi plume region: Evidence for the importance of coastal marsh inputs. *Aquatic Geochemistry*, *17*(4–5), 431–456. https://doi.org/10.1007/s10498-010-9110-3

Biscaye, P. E. (1965). Mineralogy and sedimentation of recent deep-sea clay in the Atlantic Ocean and adjacent seas and oceans. *The Geological Society of America Bulletin*, *76*(7), 803–832. https://doi.org/10.1130/0016-7606(1965)76[803:MASORD]2.0.CO;2

Blair, N. E., & Aller, R. C. (2012). The fate of terrestrial organic carbon in the marine environment. *Annual Review of Marine Science*, *4*(1), 401–423. https://doi.org/10.1146/annurev-marine-120709-142717

Blattmann, T. M., Liu, Z., Zhang, Y., Zhao, Y., Haghipour, N., Montluçon, D. B., et al. (2019). Mineralogical control on the fate of continentally derived organic matter in the ocean. *Science*, *366*(6466), 742–745. https://doi.org/10.1126/science.aax5345

Bradley, W. F. (1945). Molecular associations between montmorillonite and some polyfunctional organic liquids1. *Journal of the American Chemical Society*, *67*(6), 975–981. https://doi.org/10.1021/ja01222a028

Bray, E., & Evans, E. (1961). Distribution of n-paraffins as a clue to recognition of source beds. *Geochimica et Cosmochimica Acta*, *22*(1), 2–15. https://doi.org/10.1016/0016-7037(61)90069-2

Brockamp, O. (2011). Delamination of smectite in river-borne suspensions at the fluvial/marine interface–An experimental study. *Estuarine, Coastal and Shelf Science*, *91*(1), 33–41. https://doi.org/10.1016/j.ecss.2010.10.006

Bröder, L., Tesi, T., Andersson, A., Semiletov, I., & Gustafsson, Ö. (2018). Bounding cross-shelf transport time and degradation in Siberian-Arctic land-ocean carbon transfer. *Nature Communications*, *9*(1), 1–8. https://doi.org/10.1038/s41467-018-03192-1

Bröder, L., Tesi, T., Salvadó, J. A., Semiletov, I. P., Dudarev, O. V., & Gustafsson, Ö. (2016). Fate of terrigenous organic matter across the Laptev Sea from the mouth of the Lena River to the deep sea of the Arctic interior. *Biogeosciences*, *13*(17), 5003–5019. https://doi.org/10.5194/bg-13-5003-2016

Brunauer, S., Emmett, P. H., & Teller, E. (1938). Adsorption of gases in multimolecular layers. *Journal of the American Chemical Society*, *60*(2), 309–319. https://doi.org/10.1021/ja01269a023

Carroll, D. (1959). Ion exchange in clays and other minerals. *The Geological Society of America Bulletin*, *70*(6), 749–779. https://doi.org/10.1130/0016-7606(1959)70[749:IEICAO]2.0.CO;2

Castellini, E., Berthold, C., Malferrari, D., & Bernini, F. (2013). Sodium hexametaphosphate interaction with 2: 1 clay minerals illite and montmorillonite. *Applied Clay Science*, *83*, 162–170. https://doi.org/10.1016/j.clay.2013.08.031

Chen, M., & Diao, G. (2011). Intermolecular complexation between p-sulfonated calix [4, 6, 8] arene sodium and neutral red. *Journal of Solution Chemistry*, *40*(3), 481–491. https://doi.org/10.1007/s10953-011-9660-z

Chen, P., Wei, Y., Wei, L., Wu, H., Bu, H., Wang, G., & Wang, S. (2020). Quantitative assessments of organic matter uncoupling from clay surfaces in presence of salinity. *Applied Clay Science*, *188*, 105532. https://doi.org/10.1016/j.clay.2020.105532

Coppola, L., Gustafsson, Ö., Andersson, P., Eglinton, T., Uchida, M., & Dickens, A. (2007). The importance of ultrafine particles as a control on the distribution of organic carbon in Washington Margin and Cascadia Basin sediments. *Chemical Geology*, *243*(1–2), 142–156. https://doi.org/10.1016/j.chemgeo.2007.05.020

Corbett, D. R., McKee, B., & Allison, M. (2006). Nature of decadal-scale sediment accumulation on the western shelf of the Mississippi River delta. *Continental Shelf Research*, *26*(17–18), 2125–2140. https://doi.org/10.1016/j.csr.2006.07.012

Dearing Crampton-Flood, E., Peterse, F., & Sinninghe Damsté, J. S. (2019). Production of branched tetraethers in the marine realm: Svalbard fjord sediments revisited. *Organic Geochemistry*, *138*, 103907. https://doi.org/10.1016/j.orggeochem.2019.103907

Dickens, A. F., Baldock, J. A., Smernik, R. J., Wakeham, S. G., Arnarson, T. S., Gélinas, Y., & Hedges, J. I. (2006). Solid-state 13C NMR analysis of size and density fractions of marine sediments: Insight into organic carbon sources and preservation mechanisms. *Geochimica et Cosmochimica Acta*, *70*(3), 666–686. https://doi.org/10.1016/j.gca.2005.10.024

Dinis, P. A., Garzanti, E., Hahn, A., Vermeesch, P., & Cabral-Pinto, M. (2020). Weathering indices as climate proxies. A step forward based on Congo and SW African river muds. *Earth-Science Reviews*, *201*, 103039. https://doi.org/10.1016/j.earscirev.2019.103039

Dong, H., Zeng, Q., Sheng, Y., Chen, C., Yu, G., & Kappler, A. (2023). Coupled iron cycling and organic matter transformation across redox interfaces. *Nature Reviews Earth and Environment*, *4*(9), 659–673. https://doi.org/10.1038/s43017-023-00470-5

Drever, J. I. (1973). The preparation of oriented clay mineral specimens for X-ray diffraction analysis by a filter-membrane peel technique. *American Mineralogist: Journal of Earth and Planetary Materials*, *58*(5–6), 553–554.

Eglinton, G., & Hamilton, R. J. (1967). Leaf Epicuticular Waxes: The waxy outer surfaces of most plants display a wide diversity of fine structure and chemical constituents. *Science*, *156*(3780), 1322–1335. https://doi.org/10.1126/science.156.3780.1322

Feng, X., Simpson, A. J., & Simpson, M. J. (2005). Chemical and mineralogical controls on humic acid sorption to clay mineral surfaces. *Organic Geochemistry*, *36*(11), 1553–1566. https://doi.org/10.1016/j.orggeochem.2005.06.008

Freymond, C. V., Kündig, N., Stark, C., Peterse, F., Buggle, B., Lupker, M., et al. (2018). Evolution of biomolecular loadings along a major river system. *Geochimica et Cosmochimica Acta*, *223*, 389–404. https://doi.org/10.1016/j.gca.2017.12.010

Galy, V., Eglinton, T., France-Lanord, C., & Sylva, S. (2011). The provenance of vegetation and environmental signatures encoded in vascular plant biomarkers carried by the Ganges–Brahmaputra Rivers. *Earth and Planetary Science Letters*, *304*(1–2), 1–12. https://doi.org/10.1016/j.epsl.2011.02.003

Gelin, F., Boogers, I., Noordeloos, A. A., Damsté, J. S., de Hatcher, P., & de Leeuw, J. W. (1996). Novel, resistant microalgal polyethers: An important sink of organic carbon in the marine environment? *Geochimica et Cosmochimica Acta*, *60*(7), 1275–1280. https://doi.org/10.1016/0016-7037(96)00038-5

Goñi, M. A., Ruttenberg, K. C., & Eglinton, T. I. (1997). Sources and contribution of terrigenous organic carbon to surface sediments in the Gulf of Mexico. *Nature*, *389*(6648), 275–278. https://doi.org/10.1038/38477

Gordon, E. S., & Goñi, M. A. (2003). Sources and distribution of terrigenous organic matter delivered by the Atchafalaya River to sediments in the northern Gulf of Mexico. *Geochimica et Cosmochimica Acta*, *67*(13), 2359–2375. https://doi.org/10.1016/S0016-7037(02)01412-6

Hedges, J., & Oades, J. (1997). Comparative organic geochemistries of soils and marine sediments. *Organic Geochemistry*, *27*(7–8), 319–361. https://doi.org/10.1016/S0146-6380(97)00056-9

Hedges, J. I., & Keil, R. G. (1995). Sedimentary organic matter preservation: An assessment and speculative synthesis. *Marine Chemistry*, *49*(2–3), 81–115. https://doi.org/10.1016/0304-4203(95)00008-F

Hedges, J. I., Keil, R. G., & Benner, R. (1997). What happens to terrestrial organic matter in the ocean? *Organic Geochemistry*, *27*(5–6), 195–212. https://doi.org/10.1016/S0146-6380(97)00066-1

Hemingway, J. D., Rothman, D. H., Grant, K. E., Rosengard, S. Z., Eglinton, T. I., Derry, L. A., & Galy, V. V. (2019). Mineral protection regulates long-term global preservation of natural organic carbon. *Nature*, *570*(7760), 228–231. https://doi.org/10.1038/s41586-019-1280-6

Hoefs, M. J., Rijpstra, W. I. C., & Damsté, J. S. S. (2002). The influence of oxic degradation on the sedimentary biomarker record I: Evidence from Madeira Abyssal Plain turbidites. *Geochimica et Cosmochimica Acta*, *66*(15), 2719–2735. https://doi.org/10.1016/S0016-7037(02)00864-5

Hopmans, E. C., Schouten, S., & Sinninghe Damsté, J. S. (2016). The effect of improved chromatography on GDGT-based palaeoproxies. *Organic Geochemistry*, *93*, 1–6. https://doi.org/10.1016/j.orggeochem.2015.12.006

Hopmans, E. C., Weijers, J. W., Schefuß, E., Herfort, L., Sinninghe Damsté, J. S., & Schouten, S. (2004). A novel proxy for terrestrial organic matter in sediments based on branched and isoprenoid tetraether lipids. *Earth and Planetary Science Letters*, *224*(1–2), 107–116. https://doi.org/10.1016/j.epsl.2004.05.012

Hou, P., Yu, M., Zhao, M., Montluçon, D. B., Su, C., & Eglinton, T. I. (2020). Terrestrial biomolecular burial efficiencies on continental margins. *Journal of Geophysical Research: Biogeosciences*, *125*(8). https://doi.org/10.1029/2019JG005520

Ito, A., & Wagai, R. (2017). Global distribution of clay-size minerals on land surface for biogeochemical and climatological studies. *Scientific Data*, *4*(1), 1–11. https://doi.org/10.1038/sdata.2017.103

Jong, D., Bröder, L., Tesi, T., Keskitalo, K. H., Zimov, N., Davydova, A., et al. (2023). Contrasts in dissolved, particulate, and sedimentary organic carbon from the Kolyma River to the East Siberian shelf. *Biogeosciences*, *20*(1), 271–294. https://doi.org/10.5194/bg-20-271-2023

Karatapanis, A. E., Fiamegos, Y. C., & Stalikas, C. D. (2011). A revisit to the retention mechanism of hydrophilic interaction liquid chromatography using model organic compounds. *Journal of Chromatography A*, *1218*(20), 2871–2879. https://doi.org/10.1016/j.chroma.2011.02.069

Keil, R., & Mayer, L. (2014). Mineral matrices and organic matter. *Treatise on Geochemistry*, *12*, 337–359. https://doi.org/10.1016/B978-0-08-095975-7.01024-X

Keil, R. G., Mayer, L. M., Quay, P. D., Richey, J. E., & Hedges, J. I. (1997). Loss of organic matter from riverine particles in deltas. *Geochimica et Cosmochimica Acta*, *61*(7), 1507–1511. https://doi.org/10.1016/S0016-7037(97)00044-6

Keil, R. G., Montluçon, D. B., Prahl, F. G., & Hedges, J. I. (1994a). Sorptive preservation of labile organic matter in marine sediments. *Nature*, *370*(6490), 549–552. https://doi.org/10.1038/370549a0

Keil, R. G., Tsamakis, E., Fuh, C. B., Giddings, J. C., & Hedges, J. I. (1994b). Mineralogical and textural controls on the organic composition of coastal marine sediments: Hydrodynamic separation using SPLITT-fractionation. *Geochimica et Cosmochimica Acta*, *58*(2), 879–893. https://doi.org/10.1016/0016-7037(94)90512-6

Kennedy, M. J., & Wagner, T. (2011). Clay mineral continental amplifier for marine carbon sequestration in a greenhouse ocean. *Proceedings of the National Academy of Sciences* (Vol. 108(24), 9776–9781). https://doi.org/10.1073/pnas.1018670108

Kirkels, F. M., Ponton, C., Galy, V., West, A. J., Feakins, S. J., & Peterse, F. (2020). From Andes to Amazon: Assessing branched tetraether lipids as tracers for soil organic carbon in the Madre de Dios River system. *Journal of Geophysical Research: Biogeosciences*, *125*(1), e2019JG005270. https://doi.org/10.1029/2019JG005270

Kirkels, F. M., Zwart, H. M., Usman, M. O., Hou, S., Ponton, C., Giosan, L., et al. (2022). From soil to sea: Sources and transport of organic carbon traced by tetraether lipids in the monsoonal Godavari River, India. *Biogeosciences*, *19*(17), 3979–4010. https://doi.org/10.5194/bg-19-3979-2022

Kleber, M., Bourg, I. C., Coward, E. K., Hansel, C. M., Myneni, S. C., & Nunan, N. (2021). Dynamic interactions at the mineral–organic matter interface. *Nature Reviews Earth and Environment*, *2*(6), 402–421. https://doi.org/10.1038/s43017-021-00162-y

Kögel-Knabner, I., Guggenberger, G., Kleber, M., Kandeler, E., Kalbitz, K., Scheu, S., et al. (2008). Organo-mineral associations in temperate soils: Integrating biology, mineralogy, and organic matter chemistry. *Journal of Plant Nutrition and Soil Science*, *171*(1), 61–82. https://doi.org/10.1002/jpln.200700048

Kusch, S., Mollenhauer, G., Willmes, C., Hefter, J., Eglinton, T. I., & Galy, V. (2021). Controls on the age of plant waxes in marine sediments–a global synthesis. *Organic Geochemistry*, *157*, 104259. https://doi.org/10.1016/j.orggeochem.2021.104259

Kusch, S., Sepúlveda, J., & Wakeham, S. G. (2019). Origin of sedimentary BHPs along a Mississippi river–gulf of Mexico export transect: Insights from spatial and density distributions. *Frontiers in Marine Science*, *6*, 729. https://doi.org/10.3389/fmars.2019.00729

Lalonde, K., Mucci, A., Ouellet, A., & Gélinas, Y. (2012). Preservation of organic matter in sediments promoted by iron. *Nature*, *483*(7388), 198–200. https://doi.org/10.1038/nature10855

Largeau, C., Derenne, S., Casadevall, E., Kadouri, A., & Sellier, N. (1986). Pyrolysis of immature Torbanite and of the resistant biopolymer (PRB A) isolated from extant alga Botryococcus braunii. Mechanism of formation and structure of Torbanite. *Organic Geochemistry*, *10*(4–6), 1023–1032. https://doi.org/10.1016/s0146-6380(86)80041-9

LaRowe, D. E., Arndt, S., Bradley, J. A., Estes, E. R., Hoarfrost, A., Lang, S. Q., et al. (2020). The fate of organic carbon in marine sediments—New insights from recent data and analysis. *Earth-Science Reviews*, *204*, 103146. https://doi.org/10.1016/j.earscirev.2020.103146

Lattaud, J., Balzano, S., van der Meer, M. T., Villanueva, L., Hopmans, E. C., Sinninghe Damsté, J. S., & Schouten, S. (2021). Sources and seasonality of long-chain diols in a temperate lake (Lake Geneva). *Organic Geochemistry*, *156*, 104223. https://doi.org/10.1016/j.orggeochem.2021.104223

Lattaud, J., Eglinton, T. I., Tallon, M., Bröder, L., Erdem, Z., & Ausín, B. (2022). Grain size controls on long-chain diol distributions and proxy signals in marine sediments. *Frontiers in Marine Science*, *9*, 1004096. https://doi.org/10.3929/ethz-b-000578748

Lattaud, J., Erdem, Z., Weiss, G. M., Rush, D., Balzano, S., Chivall, D., et al. (2019). Hydrogen isotopic ratios of long-chain diols reflect salinity. *Organic Geochemistry*, *137*, 103904. https://doi.org/10.1016/j.orggeochem.2019.103904

Lattaud, J., Kim, J.-H., De Jonge, C., Zell, C., Sinninghe Damsté, J. S., & Schouten, S. (2017). The C 32 alkane-1,15-diol as a tracer for riverine input in coastal seas. *Geochimica et Cosmochimica Acta*, *202*, 146–158. https://doi.org/10.1016/j.gca.2016.12.030

Lavallee, J. M., Soong, J. L., & Cotrufo, M. F. (2020). Conceptualizing soil organic matter into particulate and mineral-associated forms to address global change in the 21st century. *Global Change Biology*, *26*(1), 261–273. https://doi.org/10.1111/gcb.14859

Lenstra, W. K., van Helmond, N. A., Żygadłowska, O. M., Van Zummeren, R., Witbaard, R., & Slomp, C. P. (2022). Sediments as a source of iron, manganese, cobalt and nickel to continental shelf waters (Louisiana, Gulf of Mexico). *Frontiers in Marine Science*, *23*. https://doi.org/10.3389/fmars.2022.81195

Liu, S., Shi, X., Fang, X., Dou, Y., Liu, Y., & Wang, X. (2014). Spatial and temporal distributions of clay minerals in mud deposits on the inner shelf of the East China Sea: Implications for paleoenvironmental changes in the Holocene. *Quaternary International*, *349*, 270–279. https://doi.org/10.1016/j.quaint.2014.07.016

Lützow, M. v., Kögel-Knabner, I., Ekschmitt, K., Matzner, E., Guggenberger, G., Marschner, B., & Flessa, H. (2006). Stabilization of organic matter in temperate soils: Mechanisms and their relevance under different soil conditions - A review: Mechanisms for organic matter stabilization in soils. *European Journal of Soil Science*, *57*(4), 426–445. https://doi.org/10.1111/j.1365-2389.2006.00809.x

Marzi, R., Torkelson, B., & Olson, R. (1993). A revised carbon preference index. *Organic Geochemistry*, *20*(8), 1303–1306. https://doi.org/10.1016/0146-6380(93)90016-5

Mayer, L. M. (1994a). Relationships between mineral surfaces and organic carbon concentrations in soils and sediments. *Chemical Geology*, *114*(3–4), 347–363. https://doi.org/10.1016/0009-2541(94)90063-9

Mayer, L. M. (1994b). Surface area control of organic carbon accumulation in continental shelf sediments. *Geochimica et Cosmochimica Acta*, *58*(4), 1271–1284. https://doi.org/10.1016/0016-7037(94)90381-6

Meade, R. H., & Moody, J. A. (2009). Causes for the decline of suspended-sediment discharge in the Mississippi River system, 1940-2007. *Hydrological Processes*, *24*(1), 35–49. https://doi.org/10.1002/hyp.7477

Mikutta, R., Schaumann, G. E., Gildemeister, D., Bonneville, S., Kramer, M. G., Chorover, J., et al. (2009). Biogeochemistry of mineral–organic associations across a long-term mineralogical soil gradient (0.3–4100 kyr), Hawaiian Islands. *Geochimica et Cosmochimica Acta*, *73*(7), 2034–2060. https://doi.org/10.1016/j.gca.2008.12.028

Neill, C. F., & Allison, M. A. (2005). Subaqueous deltaic formation on the Atchafalaya shelf, Louisiana. *Marine Geology*, *214*(4), 411–430. https://doi.org/10.1016/j.margeo.2004.11.002

Ostrom, M. E. (1961). Separation of clay minerals from carbonate rocks by using acid. *Journal of Sedimentary Research*, *31*(1), 123–129. https://doi.org/10.1306/74D70B1E-2B21-11D7-8648000102C1865D

Ponton, C., Giosan, L., Eglinton, T. I., Fuller, D. Q., Johnson, J. E., Kumar, P., & Collett, T. S. (2012). Holocene aridification of India. *Geophysical Research Letters*, *39*(3). https://doi.org/10.1029/2011GL050722

Poppe, L., Fredericks, J., & Hathaway, J. (1988). A computer program to calculate centrifugation parameters for sedimentation analyses. *Computers and Geosciences*, *14*(4), 541–545. https://doi.org/10.1016/0098-3004(88)90034-9

Poynter, J., Farrimond, P., Robinson, N., & Eglinton, G. (1989). Aeolian-derived higher plant lipids in the marine sedimentary record: Links with palaeoclimate. In *Paleoclimatology and paleometeorology: Modern and past patterns of global atmospheric transport* (pp. 435–462). Springer. https://doi.org/10.1007/978-94-009-0995-3_18

Quenea, K., Derenne, S., Largeau, C., Rumpel, C., & Mariotti, A. (2004). Variation in lipid relative abundance and composition among different particle size fractions of a forest soil. *Organic Geochemistry*, *35*(11–12), 1355–1370. https://doi.org/10.1016/j.orggeochem.2004.03.010

Rabalais, N. N., Turner, R. E., & Scavia, D. (2002). Beyond science into policy: Gulf of Mexico hypoxia and the Mississippi river. *BioScience*, *52*(2), 129–142. https://doi.org/10.1641/0006-3568(2002)052[0129:BSIPGO]2.0.CO;2

Rampen, S. W., Willmott, V., Kim, J.-H., Uliana, E., Mollenhauer, G., Schefuß, E., et al. (2012). Long chain 1,13- and 1,15-diols as a potential proxy for palaeotemperature reconstruction. *Geochimica et Cosmochimica Acta*, *84*, 204–216. https://doi.org/10.1016/j.gca.2012.01.024

Ransom, B., Kim, D., Kastner, M., & Wainwright, S. (1998). Organic matter preservation on continental slopes: Importance of mineralogy and surface area. *Geochimica et Cosmochimica Acta*, *62*(8), 1329–1345. https://doi.org/10.1016/S0016-7037(98)00050-7

Reiche, S., Rampen, S. W., Dorhout, D. J., Damsté, J. S. S., & Schouten, S. (2018). The impact of oxygen exposure on long-chain alkyl diols and the long chain diol index (LDI)–a long-term incubation study. *Organic Geochemistry*, *124*, 238–246. https://doi.org/10.1016/j.orggeochem.2018.08.003

Repasch, M., Scheingross, J. S., Hovius, N., Vieth-Hillebrand, A., Mueller, C. W., Höschen, C., et al. (2022). River organic carbon fluxes modulated by hydrodynamic sorting of particulate organic matter. *Geophysical Research Letters*, *49*(3), e2021GL096343. https://doi.org/10.1029/2021GL096343

Reuss, M. (2004). *Designing the bayous: The control of water in the Atchafalaya basin, 1800-1995 (issue 4)*. Texas A&M University Press. https://doi.org/10.2307/27649250

Reynolds, R. (1989). Principles and techniques of quantitative analysis of clay minerals by X-ray powder diffraction. *Quantitative Mineral Analysis of Clays*, 3–36. https://doi.org/10.1346/CMS-WLS-1.1

Saidy, A., Smernik, R., Baldock, J. A., Kaiser, K., & Sanderman, J. (2013). The sorption of organic carbon onto differing clay minerals in the presence and absence of hydrous iron oxide. *Geoderma*, *209*, 15–21. https://doi.org/10.1016/j.geoderma.2013.05.026

Sampere, T. P., Bianchi, T. S., Wakeham, S. G., & Allison, M. A. (2008). Sources of organic matter in surface sediments of the Louisiana Continental margin: Effects of major depositional/transport pathways and Hurricane Ivan. *Continental Shelf Research*, *28*(17), 2472–2487. https://doi.org/10.1016/j.csr.2008.06.009

Scheingross, J. S., Hovius, N., Dellinger, M., Hilton, R. G., Repasch, M., Sachse, D., et al. (2019). Preservation of organic carbon during active fluvial transport and particle abrasion. *Geology*, *47*(10), 958–962. https://doi.org/10.1130/G46442.1

Shimokawara, M., Nishimura, M., Matsuda, T., Akiyama, N., & Kawai, T. (2010). Bound forms, compositional features, major sources and diagenesis of long chain, alkyl mid-chain diols in Lake Baikal sediments over the past 28,000 years. *Organic Geochemistry*, *41*(8), 753–766. https://doi.org/10.1016/j.orggeochem.2010.05.013

Sinninghe Damsté, J. S. (2016). Spatial heterogeneity of sources of branched tetraethers in shelf systems: The geochemistry of tetraethers in the Berau River delta (Kalimantan, Indonesia). *Geochimica et Cosmochimica Acta*, *186*, 13–31. https://doi.org/10.1016/j.gca.2016.04.033

Sinninghe Damsté, J. S., Hopmans, E. C., Pancost, R. D., Schouten, S., & Geenevasen, J. A. (2000). Newly discovered non-isoprenoid glycerol dialkyl glycerol tetraether lipids in sediments. *Chemical Communications*, *17*, 1683–1684. https://doi.org/10.1039/B004517I

Sionneau, T., Bout-Roumazeilles, V., Biscaye, P., van Vliet-Lanoë, B., & Bory, A. (2008). Clay mineral distributions in and around the Mississippi River watershed and Northern Gulf of Mexico: Sources and transport patterns. *Quaternary Science Reviews*, *27*(17–18), 1740–1751. https://doi.org/10.1016/j.quascirev.2008.07.001

Suh, Y. J., Diefendorf, A. F., Bowen, G. J., Cotton, J. M., & Ju, S.-J. (2019). Plant wax integration and transport from the Mississippi River Basin to the Gulf of Mexico inferred from GIS-enabled isoscapes and mixing models. *Geochimica et Cosmochimica Acta*, *257*, 131–149. https://doi.org/10.1016/j.gca.2019.04.022

Svedberg, T., & Nichols, J. B. (1923). Determination of size and distribution of size of particle by centrifugal methods. *Journal of the American Chemical Society*, *45*(12), 2910–2917. https://doi.org/10.1021/ja01665a016

Tesi, T., Semiletov, I., Dudarev, O., Andersson, A., & Gustafsson, Ö. (2016). Matrix association effects on hydrodynamic sorting and degradation of terrestrial organic matter during cross-shelf transport in the Laptev and East Siberian shelf seas. *Journal of Geophysical Research: Biogeosciences*, *121*(3), 731–752. https://doi.org/10.1002/2015JG003067

Tesi, T., Semiletov, I., Hugelius, G., Dudarev, O., Kuhry, P., & Gustafsson, Ö. (2014). Composition and fate of terrigenous organic matter along the Arctic land–ocean continuum in East Siberia: Insights from biomarkers and carbon isotopes. *Geochimica et Cosmochimica Acta*, *133*, 235–256. https://doi.org/10.1016/j.gca.2014.02.045

Theng, B. K. G. (2012). *Formation and properties of clay-polymer complexes* (2nd ed.). Elsevier.

Trask, P. D. (1930). Mechanical analyses of sediments by centrifuge. *Economic Geology*, *25*(6), 581–599. https://doi.org/10.2113/gsecongeo.25.6.581

Trefry, J. H., Metz, S., Nelsen, T. A., Trocine, R. P., & Eadie, B. J. (1994). Transport of particulate organic carbon by the Mississippi River and its fate in the Gulf of Mexico. *Estuaries*, *17*(4), 839–849. https://doi.org/10.2307/1352752

Treignier, C., Derenne, S., & Saliot, A. (2006). Terrestrial and marine n-alcohol inputs and degradation processes relating to a sudden turbidity current in the Zaire canyon. *Organic Geochemistry*, *37*(9), 1170–1184. https://doi.org/10.1016/j.orggeochem.2006.03.010

Usman, M. O., Kirkels, F. M. S. A., Zwart, H. M., Basu, S., Ponton, C., Blattmann, T. M., et al. (2018). Reconciling drainage and receiving basin signatures of the Godavari River system. *Biogeosciences*, *15*(11), 3357–3375. https://doi.org/10.5194/bg-15-3357-2018

van der Voort, T. S., Zell, C., Hagedorn, F., Feng, X., McIntyre, C., Haghipour, N., et al. (2017). Diverse soil carbon dynamics expressed at the molecular level. *Geophysical Research Letters*, *44*(23), 11–840. https://doi.org/10.1002/2017GL076188

Volkman, J. K., Barrett, S. M., & Blackburn, S. I. (1999). Eustigmatophyte microalgae are potential sources of C29 sterols, C22–C28 n-alcohols and C28–C32 n-alkyl diols in freshwater environments. *Organic Geochemistry*, *30*(5), 307–318. https://doi.org/10.1016/S0146-6380(99)00009-1

Volkman, J. K., Barrett, S. M., Dunstan, G. A., & Jeffrey, S. (1992). C30-C32 alkyl diols and unsaturated alcohols in microalgae of the class Eustigmatophyceae. *Organic Geochemistry*, *18*(1), 131–138. https://doi.org/10.1016/0146-6380(92)90150-V

Wakeham, S. G., Canuel, E. A., Lerberg, E. J., Mason, P., Sampere, T. P., & Bianchi, T. S. (2009). Partitioning of organic matter in continental margin sediments among density fractions. *Marine Chemistry*, *115*(3–4), 211–225. https://doi.org/10.1016/j.marchem.2009.08.005

Walker, N. D., Wiseman Jr, W. J., Rouse Jr, L. J., & Babin, A. (2005). Effects of river discharge, wind stress, and slope eddies on circulation and the satellite-observed structure of the Mississippi River plume. *Journal of Coastal Research*, *21*(6), 1228–1244. https://doi.org/10.2112/04-0347.1

Wang, J., Zhao, B., Yao, P., Bianchi, T. S., Lipp, J. S., Elvert, M., et al. (2024). Size-fractionated distribution of glycerol dialkyl glycerol tetraether core lipids in surface sediments of a large-river delta-front estuary. *The Science of the Total Environment*, *912*, 169626. https://doi.org/10.1016/j.scitotenv.2023.169626

Ware, S. A., Hartman, B. E., Waggoner, D. C., Vaughn, D. R., Bianchi, T. S., & Hatcher, P. G. (2022). Molecular evidence for the export of terrigenous organic matter to the north Gulf of Mexico by solid-state 13C NMR and Fourier transform ion cyclotron resonance mass spectrometry of humic acids. *Geochimica et Cosmochimica Acta*, *317*, 39–52. https://doi.org/10.1016/j.gca.2021.10.018

Waterson, E. J., & Canuel, E. A. (2008). Sources of sedimentary organic matter in the Mississippi River and adjacent Gulf of Mexico as revealed by lipid biomarker and δ13CTOC analyses. *Organic Geochemistry*, *39*(4), 422–439. https://doi.org/10.1016/j.orggeochem.2008.01.011

Wattel-Koekkoek, E., Van Genuchten, P., Buurman, P., & Van Lagen, B. (2001). Amount and composition of clay-associated soil organic matter in a range of kaolinitic and smectitic soils. *Geoderma*, *99*(1–2), 27–49. https://doi.org/10.1016/S0016-7061(00)00062-8

Wei, L., Bu, H., Wei, Y., Wu, H., Wang, G., Chen, P., & Li, H. (2021). Fractionation of natural algal organic matter and its preservation on the surfaces of clay minerals. *Applied Clay Science*, *213*, 106235. https://doi.org/10.1016/j.clay.2021.106235

Weijers, J. W., Schouten, S., Schefuß, E., Schneider, R. R., & Damste, J. S. S. (2009). Disentangling marine, soil and plant organic carbon contributions to continental margin sediments: A multi-proxy approach in a 20,000 year sediment record from the Congo deep-sea fan. *Geochimica et Cosmochimica Acta*, *73*(1), 119–132. https://doi.org/10.1016/j.gca.2008.10.016

Wentworth, C. K. (1922). A scale of grade and class terms for clastic sediments. *The Journal of Geology*, *30*(5), 377–392. https://doi.org/10.1086/622910

Yedema, Y. W., Sangiorgi, F., Sluijs, A., Sinninghe Damsté, J. S., & Peterse, F. (2023). The dispersal of fluvially discharged and marine, shelf-produced particulate organic matter in the northern Gulf of Mexico. *Biogeosciences*, *20*(3), 663–686. https://doi.org/10.5194/bg-20-663-2023

Yu, M., Eglinton, T. I., Haghipour, N., Montluçon, D. B., Wacker, L., Hou, P., et al. (2021). Contrasting fates of terrestrial organic carbon pools in marginal sea sediments. *Geochimica et Cosmochimica Acta*, *309*, 16–30. https://doi.org/10.1016/j.gca.2021.06.018

Yu, M., Zhang, H., Li, L., & Zhao, M. (2018). Spatial distributions and potential sources of long chain (C 30, C 32 1, 15-) alkyl diols in surface sediments from Eastern China Marginal Seas. *Journal of Ocean University of China*, *17*(5), 1114–1122. https://doi.org/10.1007/s11802-018-3686-4

Zell, C., Kim, J.-H., Balsinha, M., Dorhout, D., Fernandes, C., Baas, M., & Sinninghe Damsté, J. S. (2014a). Transport of branched tetraether lipids from the Tagus River basin to the coastal ocean of the Portuguese margin: Consequences for the interpretation of the MBT'/CBT paleothermometer. *Biogeosciences*, *11*(19), 5637–5655. https://doi.org/10.5194/bg-11-5637-2014

Zell, C., Kim, J.-H., Hollander, D., Lorenzoni, L., Baker, P., Silva, C. G., et al. (2014b). Sources and distributions of branched and isoprenoid tetraether lipids on the Amazon shelf and fan: Implications for the use of GDGT-based proxies in marine sediments. *Geochimica et Cosmochimica Acta*, *139*, 293–312. https://doi.org/10.1016/j.gca.2014.04.038

Zhao, B., Yao, P., Bianchi, T. S., Shields, M. R., Cui, X., Zhang, X., et al. (2018). The role of reactive iron in the preservation of terrestrial organic carbon in estuarine sediments. *Journal of Geophysical Research: Biogeosciences*, *123*(12), 3556–3569. https://doi.org/10.1029/2018JG004649

Zhao, T., Xu, S., & Hao, F. (2023). Differential adsorption of clay minerals: Implications for organic matter enrichment. *Earth-Science Reviews*, *104598*, 104598. https://doi.org/10.1016/j.earscirev.2023.104598

Zhou, J. L., Rowland, S., Fauzi, R., Mantoura, C., & Braven, J. (1994). The formation of humic coatings on mineral particles under simulated estuarine conditions—A mechanistic study. *Water Research*, *28*(3), 571–579. https://doi.org/10.1016/0043-1354(94)90008-6